BETA DOSIMETRY:

THE SCALING METHOD FOR BETA-RAY DOSE DISTRIBUTIONS APPLIED TO LAYERED MEDIA

BETA DOSIMETRY:

THE SCALING METHOD FOR BETA-RAY DOSE DISTRIBUTIONS APPLIED TO LAYERED MEDIA

By

SILVIU-MARCEL MARCU, B.Sc.

A Thesis

Submitted to the School of Graduate Studies

in Partial Fulfillment of the Requirements

for the Degree

Master of Science

McMaster University

© Copyright by Silviu-Marcel Marcu, September 1996.

MASTER OF SCIENCE (1996) McMaster University
(Physics) Hamilton, Ontario

TITLE: Beta Dosimetry:
The Scaling Method for Beta-ray Dose Distributions

AUTHOR: Siviu-Marcel Marcu, B.Sc. (University of Bucharest)

SUPERVISOR: Professor W.V. Prestwich

NUMBER OF PAGES: xiii, 96.

McMASTER UNIVERSITY LIBRARY

ABSTRACT

Radioimmunotherapy consists in the use of beta radioactive labeled monoclonal antibodies as selective carriers of radiation to tumors. Internal spatially distributed sources created at the disease sites would deliver high radiation doses to tumors while the normal tissues would not be exposed to the intense radiation as in conventional forms of cancer treatments.

A rapid and accurate estimation of the spatial dose distribution from nonuniform sources is essential for the optimization of this form of cancer therapy. The method used for such calculations is based on the knowledge of dose distributions around a unit source, quantities referred to as dose kernels. Thus far, the Monte Carlo technique is the most accurate way of the dose kernel determinations. However, for routine dosimetry simpler and less time consuming methods of adequate accuracy may appear more preferable.

The "scaling factor" method is used to determine the depth dose distribution in a medium based on data about the dose distribution in an arbitrary reference medium (e.g. air, water). The transformation of the dose distribution curves from the reference medium to the desired new medium is done using a constant, known as scaling factor or relative dose attenuation, and a closely related renormalization factor imposed by the energy conservation.

This work investigates the accuracy of the scaling factor method using a statistical approach (generalized chi-squared test), focusing on a particular case of potential practical interest, the scaling factor water to bone. The work also investigates a procedure for extending the applicability of the scaling factor method to dosimetry in dissimilar media, as a first step, a planar interface.

ACKNOWLEDGMENTS

I would like to thank my supervisor, Dr. W.V. Prestwich , for his guidance and advice throughout this project. I am also grateful to McMaster University for the opportunity and the financial support offered.

My thanks to Dr. D. Chettle and Dr. C.S. Kwok for their help during the realization of this project.

Finally, I extend my gratitude to all my colleagues, the graduate students in medical physics, for the open and stimulating scientific environment that I have enjoyed at McMaster.

TABLE OF CONTENTS

LIST OF ILLUSTRATIONS

LIST OF TABLES

CHAPTER 1.

1. Introduction

Radioimmunotherapy is a very promising form of cancer radiation therapy. It consist in the use of radiolabeled monoclonal antibodies (MAb) as selective carriers of beta emitting radioisotopes to the tumors. Ideally, lethal doses of radiation would be delivered precisely to the areas of disease while sparing normal tissue, in contrast to the traditional external beam radiation. The method is suitable for single tumors and also for widespread metastases, which are difficult to treat by conventional modalities.

The use of antibodies for treating disease has been around since 1895 but a real breakthrough in the field of radioimmunotherapy occurred in 1975 when Köhler and Milstein developed an efficient method of producing monoclonal antibodies. The major obstacle remaining to be overcome at present is the limitation to subtherapeutic absorbed doses caused by low (and sometimes inhomogeneous) tumor uptake of the radiopharmaceutical and, by restrictions on the injected amount of radionuclide because of hematopoetic toxicity (Raylman 1995).

The accumulation of beta radioisotopes at the neoplasm site generates spatially nonuniformly distributed sources. Reliable and rapid methods of dose estimation for this specific case of spatially distributed sources are essential for this type of radiotherapy.

The concept of beta dose point kernel which, by definition, represent the dose distribution around a point source of beta emitting radionuclide of unit strength, is used for dose distribution calculations in homogeneous media. The principle of linearity allows the calculation of the dose around any intensity point source by simple multiplication of the dose point kernel with the source intensity. Dose is a scalar quantity so that, at any point, the contribution to the absorbed dose from one source element can be added independently to the contribution from another source element (superposition principle). Thus, the total dose is calculated as the sum of the contributions of each infinitesimal point source into which a spatial distributed source is decomposed. The most accurate techniques of treating the electron transport problems and implicitly of calculating beta dose deposition are based on Monte Carlo methods.

To solve the problems of routine dosimetry, it is usually unreasonable to employ the realistic and in principle precise, but very time consuming, Monte Carlo methods. Simpler empirical or semiempirical methods such as the "scaling factor" method may appear more preferable in practice, even though of limited accuracy.

The present work has two main directions. First is to investigate the accuracy of the scaling factor method using a statistical approach (generalized χ^2 test), focusing on a

particular case of potential practical interest, the scaling factor water to bone [compact bone ICRU (1964)]. The second direction is an attempt to extend the applicability of the scaling factor method to dissimilar media, as a first step, a planar source and interface. The investigation was done for a source of the radioisotope ^{32}P and an interface water-medium "i", where medium "i" could be any medium with the atomic number in the range $8<Z<50$.

CHAPTER 2.

2. Beta Dosimetry

2.1. Electron Interactions

The free electron as a particle is the lightest charged lepton and is identical to the atomic electrons with which it interacts. Electrons are produced in nature through the decay of radioisotopes in the process of β-emission, Auger electron emission, internal conversion and the photo-electric effect. The specificity of beta interactions with matter is summarized as follows:

As a charged particle, the electron interacts with both the positively charged nucleus and atomic electrons. The probability of passing through a layer of matter without any interaction is nil. Light in comparison to a nuclear mass, only a small fraction of an electron's energy is transferred, on average, through electron-nucleus interactions. These interactions, however, may lead to large accelerations of the electron in the nuclear electric field and consequently to Bremsstrahlung radiation production. Electron-electron interactions involve particles with equal masses so that large energy transfer can occur. In

addition, for this type of interaction between identical particles, exchange effects are relevant.

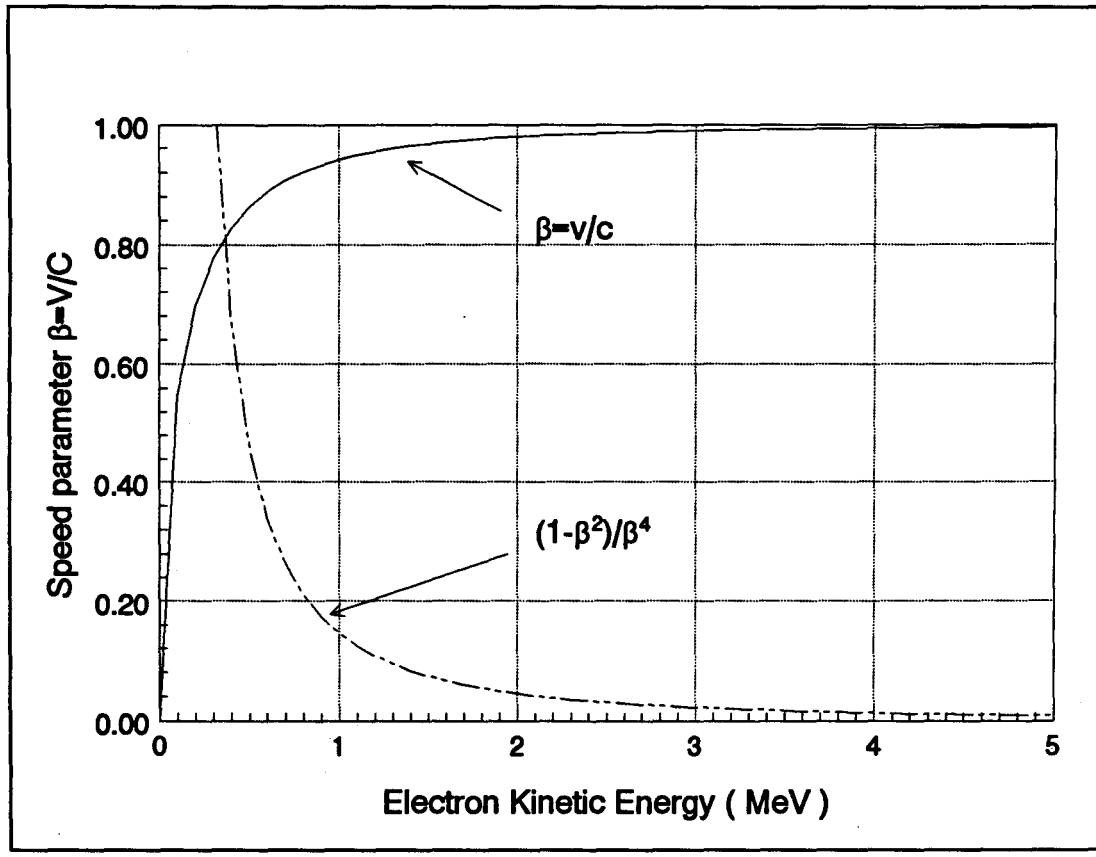

Fig.2.1 The variation of the electron speed parameter $\beta=v/c$ and the velocity term $[(1-\beta^2)/\beta^4]$ in Rutherford scattering cross-section expression (eq. 2.9) versus the electron kinetic energy.

Because the rest mass energy of an electron (0.511 MeV) is usually small in comparison to its kinetic energy, relativistic effects should be accounted for when considering electrons with energies above a few hundred of keV. The relativistic speed

parameter β, electron velocity over speed of ligh β=v/c, rises fom β=0.06 at 1keV to 0.94 at 1MeV. Fig. 2.1. shows the variation of the speed parameter β with the electron kinetic energy.

Electron interactions are categorized in term of the relative size of the impact parameter b versus the classical atom radius a. The classical impact parameter b is defined as the closest distance achieved between the line of motion of the incident particle and the center of the target atom. Three distinct cases of electron interactions are identified:

1. Soft collisions, where the electron passes an atom at a considerable distance (b>>a). The interaction is with the atom as a whole, resulting in distortion, excitation and sometime ionization of the target atoms. It is by far the most numerous type of interaction, and accounts for roughly half of the energy transferred to the absorbing medium (Attix 1986). In condensed media (liquids and solids) the atomic (dipole) distortions screen the electric field of atoms further away from the passing electron, giving rise to the polarization or density effect, and resulting in a decrease in energy loss.

2. Hard or "Knock-on" collisions, where the impact parameter is of the order of magnitude of the atomic dimensions (b≅a). The interaction is primarily with a single atomic electron which is then ejected from the atom with considerable energy as a delta (δ) ray. In the theoretical treatment the binding energy is neglected and the atomic electron is treated as "free". The ionization produced by the delta rays is denoted as

secondary ionization in contrast to the primary ionization produced by the source and primary electrons. Although hard collisions are few in number compared to soft collisions, the fractions of the primary particle's energy that are spent by these two processes are generally comparable (Attix 1986).

The collisions with atomic electrons (hard and soft) are responsible for almost all of the energy loss but their contribution to scattering is fairly small. According to Kase (1978) it is about 10% for Z=10 and 1% for Z=82.

3. Interactions with the external nuclear field, where the impact parameter is much smaller then the atomic radius (b<<a). The Coulomb force interaction takes place mainly with the nucleus. In all but 2-3% of such encounters, the electron is scattered elastically. It loses just the insignificant amount of kinetic energy necessary to satisfy conservation of momentum for the collision. This is not a mechanism for the transfer of energy but is an important means of deflecting electrons.

For the other 2-3% of the cases when the electron passes near the nucleus, an inelastic radiative interaction occurs resulting in a X-ray photon emission (bremsstrahlung). The electron may lose up to its total kinetic energy during this process. Although bremsstrahlung production is an important means of energy dissipation for energetic electrons in high-Z media, it is relatively insignificant in low-Z materials (tissue-equivalent).

2.2. Electron Transport

The passage of electrons through matter is a very complex phenomenon due to the large number of elastic and inelastic interactions resulting in scattering and energy losses. For an energy reduction from 0.5 MeV to 1keV, electrons traveling in aluminum, Andreo (1991) estimates a total number of 10^4 collisions as typical. An electron's path is tortuous and unique as a consequence of the stochastic character of the interactions. As a result the end point of the electron's path, or its range, is not distinct. This feature is described as range straggling. A related effect, energy straggling, is the spread of energies observed in an initially identical electron population after they have traversed the same path length.

Three nonstochastic quantities related to the electron range are used: the maximum range, the practical or extrapolated range and the CSDA range. The first two are defined by a beta transmission measurement. The maximum range is the absorber thickness required to reduce the beta particle transmission to the background level. The extrapolated range is given by the intersection of the linear extrapolation of the middle portion of the monoenergetic electron transmission curve with the background level (Evans 1955).

Due to the fact that electron scattering through relatively large angles occurs with significant frequency, a global approach to electron transport, energy loss and scattering together is very complicated. It is usual to approximate the situation by assuming that the interactions can be divided into inelastic collisions, in which the electron loses energy with no change in direction and, elastic scattering in which the electron changes direction

without energy loss. The first type of interaction produces the slowing down process, and, in the absence of angular deflections results in a well defined range. This is the CSDA (Continuous Slowing Down Approximation) range which is mathematically defined as:

$$R_0 = \int_0^{E_0} \frac{dE}{S(E)} \qquad (2.1)$$

Thus, the CSDA range R_0 is the distance over which the initial energy of the electron E_0 is completely exhausted. The model neglects the energy loss straggling and considers the electrons to lose energy in a deterministic continuous manner according to a stopping power function S(E). The stopping power function represents the energy lost per unit path length and is defined as:

$$S(E) = -\frac{dE}{dx} \qquad (2.2)$$

where dx is an element of path length. The quantity $\frac{1}{\rho}S(E)$ is referred to as the mass stopping power.

A. Energy Loss by Electron Inelastic Interactions

Since there are two distinctly different mechanisms of interaction leading to energy deposition, the electron stopping power may be subdivided into collision stopping power $S_c(E)$ and radiative stopping power $S_r(E)$, corresponding to the two mechanisms involved: collision and bremsstrahlung production.

$$S(E) = S_c(E) + S_r(E) \qquad (2.3)$$

The collisional stopping power is in turn the result of the sum of hard and soft collision interactions and may be written as (Attix 1986):

$$\frac{1}{\rho} S_c = k \cdot \left[\ln \frac{\tau^2(\tau+2)}{2\left(\frac{I}{mc^2}\right)^2} + F^-(\tau) - \delta - \frac{2C}{Z} \right] \qquad (2.4)$$

with: $$k = 2\pi \frac{N_A \cdot Z}{A} \cdot r_0^2 \frac{mc^2}{\beta^2}$$

and $$F^-(\tau) = 1 - \beta^2 + \frac{\frac{\tau}{8} - (2\tau+1)\ln 2}{(\tau+1)^2}$$

where r_0 is the classical electron radius, N_AZ/A is the number of electrons per gram of medium, v is the electron velocity, c is the speed of light in vacuum, β is the ratio v/c, m is the rest mass of the electron, τ is the kinetic energy of the electron in units of mc^2, I is the mean excitation and ionization potential of the absorber, δ is the correction for the density effect discussed earlier and, C/Z is the shell correction. The shell correction term 2C/Z corrects the Born approximation when the electron velocity is no longer much greater than that of the atomic electrons in the stopping medium.

The calculation of the energy loss due to the emission of bremsstrahlung is more involved than the calculation of the energy loss through collisions. None of the existing theories accurately describes the bremsstrahlung cross section over a wide range of conditions (Seltzer 1988). The mass radiative stopping power in units of MeV cm^2/g can be written as (Evans 1955):

$$\frac{1}{\rho}S_r = \sigma_0 \cdot \frac{N_A \cdot Z^2}{A}(E + mc^2)\overline{B_r} \qquad (2.5)$$

where $\sigma_0 = \frac{1}{137}(e^2 / mc^2)^2$, and $\overline{B_r}$ is a slowly varying dimensionless function of Z and electron kinetic energy E.

The following general properties of these expressions should be noted. While the collision stopping power is proportional to Z and $1/\beta^2$, the radiative stopping power is approximately proportional to E (at high energies) and Z^2 and as such, the radiative losses are more significant for high electron energies and high atomic number absorbers. The ratio of radiative to collision stopping power may be used to asses the contributions of the two mechanisms involved in energy losses. This ratio is given by (Attix 1986):

$$\frac{S_r}{S_c} = \frac{Z \cdot E}{n} \qquad (2.6)$$

where E is the kinetic energy of the particle, Z is the atomic number of the medium and n is a constant variously taken to be 700 or 800 MeV.

Another way to quantitatively characterize the contribution of the radiative energy loss process to the total electron energy loss is obtained from the radiative yield $y_{rad}(E)$. It represents the fraction of the incident electron's kinetic energy that is converted to bremsstrahlung throughout its history. An approximate relationship that gives the radiative yield is (Zerby 1967) (E is in units of mc^2):

$$y_{rad}(E) = \frac{3 \cdot 10^{-4} \cdot ZE}{1 + 3 \cdot 10^{-4} \cdot ZE} \qquad (2.7)$$

For E=694keV, the average energy of ^{32}P emitted electrons, and the highest atomic number material worked here, cadmium (Z=48), the ratio radiative over collision stopping power gives $S_r/S_c \approx 4\%$ and the radiative yields $y_{rad} \approx 2\%$.

The absorbed dose $D(\vec{r})$ is a quantity of primary interest for practical purposes and is defined as the energy per unit mass received by the absorbing medium from the radiation field. The absorbed dose at a particular point in a medium is the product of the electron fluence $\Phi(\vec{r})$ at that point and the appropriate collisional stopping power. The expression given by ICRU (35, 1984) to calculate this quantity is:

$$D(\vec{r}) = -\int_0^{E_0} \left(\frac{dE}{dx} \cdot \Phi_{E,r}(\vec{r}) + E \frac{d\Phi_{E,r}(\vec{r})}{dx} \right) \cdot dE \qquad (2.8)$$

where the first term of the integrand represents the energy deposited by the radiation field passing through the distance dx, while the second is the contribution of the electrons coming to rest in dx.

B. Scattering by Electron Elastic Interactions

Elastic nuclear scattering, or Rutherford scattering, is largely responsible for the characteristic zig-zag path of electrons penetrating a medium. Classical and quantum mechanical derivations of the Rutherford cross-section give the same result (Evans 1955):

$$\frac{d\sigma}{d\Omega} = \frac{Z^2}{4}\left(\frac{e^2}{m \cdot c^2}\right)^2 \cdot \left(\frac{1-\beta^2}{\beta^4}\right) \cdot \left(\frac{1}{\sin^4 \theta/2}\right) \qquad (2.9)$$

where β is the relativistic speed parameter (electron velocity over speed of ligh β=v/c), m is the electron rest mass, θ is the scattering angle in the laboratory system and Ω is the solid angle. The variation of the velocity term $[(1-\beta^2)/\beta^4]$ with the electron kinetic energy is shown in Fig.2.1.

The Rutherford cross section is only applicable in the case of a bare point nucleus for an electron moving at non-relativistic velocities. Mott first applied the relativistic theory of the electron to the problem of nuclear scattering, using the Bohr perturbation approximation. He obtained a general result for the differential nuclear cross section in terms of a conditionally convergent infinite series. In the case of small deflections the Mott and Rutherford scattering cross sections are equal. For larger values of deflection θ the quantum-mechanical theory gives smaller cross sections than the classical theory for all light elements (Evans 1955).

The presence of atomic electrons tends to screen the nuclear charge. In addition , the electrons constitute supplementary scattering centers. The screening effect is not

noticeable at ordinary beta ray energies (Evans 1955). The elastic electron-electron scattering cross section was also calculated by Mott using the symmetry proprieties required in the treatment of identical particles interactions. The order of magnitude of the cross section of electron scattering is the same as the nuclear scattering [$(e/mv^2)^2$, for Z=1] and increases only with Z while the nuclear scattering cross section increases with Z^2. In the theory of multiple scattering, where the statistical average of many collisions is to be evaluated, the effect of the electronic scattering can usually be included, to a satisfactory approximation, by using only the expression for nuclear single scattering, but with $(Z^2+Z)=Z(Z+1)$ instead of Z^2.

2.3. Electron Backscattering

An electron incident from one side of an interface may undergo sufficient deflection from its initial course such that it reemerges from the surface through which it entered. This is the electron backscattering phenomenon. All of the following considerations are for the case of the saturation backscattering, which in practice occurs when the thickness of backscatterer is larger than half the electron range.

Two simplifying models with limited applicability describe the backscatering phenomenon. The "Diffusion Theory" assumes that the electrons travel straight into the target up to a certain specified distance, after which they diffuse evenly in all directions.

This approach acknowledges the fact that owing to multiple collisions an electron's progress eventually becomes random, but it ignores the possibility of a large single elastic reflection. Obviously the "Large Single Elastic Theory" is the second approach which takes into consideration the presence of electrons elastically scattered through large angles, but ignores the diffusing effect of multiple collisions. Archard (1961) combined the two theories. Comparing the predictions with the experimental data, he identified three characteristic regions by scatterer atomic number. For low atomic number scatterer ($Z<11$), the large single elastic scattering predominates, while for high atomic number scatterer ($Z>60$), diffusion theory predominates. In the middle region ($11<Z<60$), the author propose the average of the two backscattering mechanisms as a good approximation.

By experimentally investigating the energetic spectrum of backscattered electrons Snyman (1963) found that the average energy of the backscattered beta rays is considerably reduced compared to the incident spectrum. The reduction is greatest for the higher energy components backscattered from elements of low atomic number. The preponderance of higher energy radiation from the higher atomic number backscatterer is attributed to a higher elastic nuclear scattering cross section. The presence of backscattered electrons at all energies up to the maximum of the incident spectrum is strong evidence of the presence of singly scattered events.

The backscattering phenomenon can be quantitatively analyzed in terms of number of electrons backscattered or of dose backscattered. The number backscatter factor B_n,

defined as the ratio of the number of reflected electrons on an interface to the number of incident electrons, was empirically found to be directly proportional with:

$$B_n \propto \sqrt{\frac{Z\cdot(Z+1)}{A}} \qquad \text{(Mladjienovic 1970)} \qquad \text{or with}$$

$$B_n \propto \log(Z+1) \qquad \text{(Baily 1980)} \qquad (2.10)$$

Due to the electrons' reflection by the backscatterer medium, an increase in dose will occur in the first medium from which the electrons are coming.

One defines the dose enhancement ratio DER as the ratio of the dose received in the presence of a scatterer to that of the homogeneous case. The dose bacscatter factor is then defined as:

$$B=DER-1 \qquad (2.11)$$

The dose backscatter factor is a spatially varying quantity. It will be of the form B(x) for a planar interface, one dimensional case, where x is the distance to the interface.

2.4. Point Dose Kernels

The dose due to a uniform source distribution is readily determined. In this case, the rate of energy delivered per unit time equals the rate of energy emitted per unit time from a beta source.

The calculation of the dose generated by a spatially distributed beta source is more complicated. The pioneering work was done by Loevinger (1950) who proposed the

use of point dose kernels for such situations. The beta dose distribution around a unit point source of the radioisotope of interest is referred to as the beta dose point kernel. In homogeneous media, the principle of linearity ensures that once the dose distribution from a unit point source is known, then the dose may by calculated for any activity. Based on experimental data, Loevinger found an empirical analytical representation of the dose point kernels for a dozen different radionuclides in air.

The first breakthrough came with the work of Spencer (1955) who solved the transport equation for electrons using a combination of analytical and numerical techniques and calculated the dose distribution around a monoenergetic unit point source in an infinite homogeneous medium, a quantity known as the monoenergetic dose point kernel. The method is the first departure from the straight line motion model and acknowledges the multiple scattering.

Integrating the monoenergetic point dose kernels over the appropriate spectrum results in the beta dose point kernel for that particular isotope. By using the superposition principle (the dose from one source element can be added independently to the contribution from another source element), the dose distribution generated by a spatial source can be simply evaluated as the convolution over the source volume of the beta dose point kernel and the spatial dose distribution. Thus, the problem of dose calculation produced by nonuniformly distributed sources reduces ultimately to the determination of monoenergetic dose kernels.

Loevinger had shown early in 1950 that beta depth-dose deposition can be determined in two geometries: point and plane giving rise to the point dose kernel J(r) and plane dose kernel I(z), respectively. In most cases the plane geometry presents advantages over the point geometry, especially in experimental work (e.g. a plane detector is practically more feasible than a point detector). The dose depositions in the two geometries are related, so that one may be derived from each other via:

$$I(z) = 2\pi \int_{z}^{+\infty} \cdot rJ(r) \cdot dr \qquad (2.12)$$

$$J(r) = \frac{1}{2\pi \cdot z} \cdot \left(- \frac{dI}{dz} \right) \qquad (2.13)$$

where r and z are the distances from the point and plane unit sources, respectively.

An important advance has been the development of a Monte Carlo method by Berger (1963) specifically designed for electron transport. Using this approach, delta rays, bremsstrahlung and the energy loss straggling were incorporated into the monoenergetic dose point kernel calculations

There has been a permanent challenge over the last twenty-five years to calculate more accurate monoenergetic dose point kernels in different media and derive dose point kernels for a variety of radionuclides of use or, of potential use, in radiotherapy. Of significance has been the work of Berger M.G. (1970, 1971, 1973), Cross W.G.(1982, 1992) and Prestwich W.V. (1985, 1989). Comparison of calculated dose distributions with experimental results shows an agreement of 3%, which is within the estimated uncertainties of the measurement and calculations (Cross 1992). By comparing the results of different Monte Carlo codes, an agreement of 2% or better is reported (Cross 1992) except near the maxima (where they amount to 3 or 4%) or near the end of the range.

One may conclude that the Monte Carlo technique is an accurate instrument of electron dose deposition investigations. Its major drawback remains the long running time required to count enough "electron histories" for good statistics.

2.5. Monte Carlo Technique

The Monte Carlo technique was created to predict outcomes for series of events, where each event has its own probability. In the context of radiation transport, the Monte Carlo technique simulates the random trajectories, or histories, of individual particles by

using machine generated (pseudo)-random numbers to sample from the probability distributions of the governing physical processes. By simulating a large number of histories, information can be obtained about average values of macroscopic quantities such as energy distribution. The Monte Carlo technique is also a very useful and unique instrument of investigation for arrangements which are not experimentally feasible.

Many problems in radiation dosimetry, radiotherapy physics, and radiation protection have been addressed by Monte Carlo technique, where analytical solutions have proven intractable due to the complexity of electron and photon interactions. Two factors have contributed in the recent years to the significant increase in the use of the technique: one is the increase in speed and decrease in cost of data processing, and the other is the availability of large, general purpose software packages.

The major problems in the Monte Carlo simulations of electron transport are the time-consuming large number of individual interactions of the primary electron, and the numerous cascades of secondary radiation comprising the electron history. The solution came by using the condensed-history method (Berger 1963). The electron trajectory is broken into a series of steps for which the effect of a large number of individual interactions occurring during a step are grouped together. Multiple scattering theories are used to determine the net angular deflection after such a step. The energy loss for the group of interactions is assessed by using either the continuous slowing down model or an energy loss distribution, such as the Landau distribution.

Monte Carlo codes can be divided into two broad categories, called class I and class II by Berger (1963). These are distinguished by how they treat individual events that lead to bremsstrahlung photons and/or knock-on electrons. In the class I models, the energy losses and angular deflections associated with all individual events are grouped together and the energy and direction of the primary electrons are not affected by the creation of individual secondary particles. In class II models, individual interactions affect the energy and direction of the primary electron when they create knock-on electrons or

bremsstrahlung photons above certain energy thresholds, although the effects of secondary particle production below these thresholds are still grouped together.

The very sophisticated Monte Carlo codes used now originated from the work of two groups of researchers. One was developed at the National Bureau of Standards by Berger and Seltzer (1973) as ETRAN (electron transport) code. The other was developed at the Stanford Linear Accelerator Center by Ford and Nelson (1978) as EGS (electron gamma shower) code (Rogers 1990). Very recently a third independent code was reported, GEPTS (gamma, electron and positron transport system) by O. Chibani (1995).

A Monte Carlo code has four major components: 1. the cross section data for all the processes being considered in the simulation, 2. the algorithm used for the particle transport, 3. the method used to specify the geometry of the problem and to determine the physical quantities of interest, and 4. the analysis of the information obtained during the simulation. The first two components comprise all the physics of the simulation.

The present work has used the TIGER code, part of the ITS (Integrated Tiger Series) derived from ETRAN. This code belongs to the class I algorithm. The ITS package includes three codes that differ primarily in their dimensional and geometric modeling. TIGER is a one-dimensional multilayer code. CYLTRAN employs a fully three dimensional description of particle trajectory within a cylindrical material geometry, and it finds application in problems involving electron or photon beam sources. ACCEPT is a general three dimensional transport code.

The version used (Version 2.1) was derived at the Sandia National Laboratory by Halbleib J.A., Mehlhorn T.A., and Kensek R.D. and uses the most recent stopping powers and bremsstrahlung cross sections data. It also contains a correction of an error in the sampling from the Landau/Blunck-Liesegang distribution of energy losses.

The codes provide output in terms of energy and charge deposition and their uncertainties in user specified zones (up to 100 scoring zones for the TIGER code). The estimation of the statistical standard error is made by dividing the total number of histories into equal batches N (by default N=10). Using the average <x> and the squared average of

the appropriate quantity $<x^2>$ per batch, the statistical standard deviation of the quantity x may be written as (Halbleib 1984):

$$\sigma_N = \sqrt{\frac{\left| < x^2 > - < x >^2 \right|}{N-1}} \qquad (2.14)$$

where: $< x >= \frac{1}{N} \cdot \sum_{i=1}^{N} x_i$ and $< x^2 >= \frac{1}{N} \cdot \sum_{i=1}^{N} x^2{}_i$

The x_i's are the value of the quantity obtained for each batch.

2.6 The Scaling Method

As mentioned in the previous sections, the Monte Carlo methods can accurately calculate electron dose deposition but have the disadvantage of being time consuming. For routine dosimetry empirical or semi-empirical methods (though of limited accuracy) may appear more preferable.

The scaling factor method is used to determine the depth dose distribution in a medium based on data about the dose distribution in an arbitrary reference medium (e.g. air , water). The method depends on the observation that beta-dose distribution in slightly different average atomic number media have very nearly the same shape. They differ by a "scaling factor" on distance and a closely related renormalization factor. This behavior has been shown by measurements on point and plane isotropic sources in both solid and gaseous media as well as by calculations based on the continuous slowing down approximation (Cross 1967, 1968,1969). . The method has often been used to convert distributions measured in air (Z_{eff}=7.36) to tissue-like media (Z_{eff}~6.5).

Theoretically approximately similar shapes are expected because, the variation with Z of both stopping power and scattering probability are nearly independent of their

variation with energy, as can be seen from Bethe's and Mott's well-known expressions for these two quantities. The scaling method should normally provide accurate results for low and similar atomic number media.

According to the method, with the indices 1 and 2 indicating the two media, the scaling relation for the plane geometry takes the form:

$$I_2(x) = \eta_{21} \cdot I_1(\eta_{21} x) \qquad (2.15)$$

where the normalizing constant is derived from the condition that the total energy deposited $E_i = \int_0^{+\infty} I_i(x)dx$ is the same in both media $E_1=E_2$, and with I_i (x) the dose in medium "i" at the depth x(g/cm^2).

For the point geometry the scaling relation is given by:

$$J_2(r) = \eta_{21}^3 \cdot \left(\frac{\rho_2}{\rho_1}\right)^2 \cdot J_1(\eta_{21} r) \qquad (2.16)$$

the normalizing factor is derived from the same condition of equal total energy deposition in both media $E_1=E_2$, with $E_i = \frac{4\pi}{\rho_i^2}\int_0^{+\infty} r^2 J_i(r)dr$, J_i(r) the dose in medium "i" at the distance r(g/cm^2), and ρ_i (g/cm^3) the density of medium "i".

The quantity η_{21} is called the "relative attenuation factor" or "scaling factor" of medium 2 relative to medium 1 (Cross 1982, 1992).

From equation (2.15) or (2.16) can be simply derived two important proprieties of the scaling factors. The scaling factor of medium 1 relative to 2 is simply the reciprocal of the scaling factor of medium 2 relative to 1:

$$\eta_{12} = \frac{1}{\eta_{21}} \qquad (2.17)$$

The scaling factors which relate three different media are not independent of each other and they satisfy the relationship:

$$\eta_{21} = \frac{\eta_{23}}{\eta_{13}} \qquad (2.18)$$

Cross (1967, 1982, 1992) has extensively investigated the scaling factor method based on experimental and calculated data. By choosing a fixed reference medium as medium 1 he found an almost linear variation of the ratio of scaling factor η_{21} over the relative stopping power (S_2/S_1) with the effective atomic number of the medium in which the dose is derived (medium 2). The empirical curves relative to air and water for low-Z ($Z<18$) materials are given in Cross (1967, 1982, 1992). For $Z>18$ the reference medium was chosen as aluminum and the linear empirical fit is given in Cross (1982).

According to Cross the scaling factor is independent of energy to within ±1%. The typical accuracy of scaling factor determination is ±1% for low-Z media and up to ±5% for Z=82.

2.7. Two-Group Method

The Two-Group method is an analytical approach dealing with beta dosimetry in heterogeneous media (Radzievsky 1982). The method can be used to calculate dose backscatter factors as a function of distance from a planar interface, which was of concern in this work.

The "Two-Group" semi-empirical method was created to estimate the dose distribution from extended or localized sources of beta radiation in heterogeneous combinations of different media with Z values and densities ρ in the approximate intervals

$7<Z<50$; $0.1<\rho<10$. The accuracy of dose determination targeted by the method's authors is to be better than 10-15%.

Fundamental to the method is that the radionuclide spectrum is described by a sum of partial quasi-equilibrium spectra. This limitation is not essential, since any emission spectrum can be expanded quite accurately as the superposition of several partial sources (Radzievsky 1980).

A rough schematic model of electron transport includes two stages generating two correspondent fluence components: directional (radial) motion, and diffusion, hence the name "Two-Group". The method consists of solving the equations which represent the two group fluence field for each partial source. The parameters, even though having physical signification, are empirically determined by fitting with experimental data. The location of the source for the diffusion component is artificially chosen to be the source position.

In accordance with the adopted way of describing the field, the fluence $\Phi(\vec{r})$ for each partial source is equal to the sum of the directional $\Phi_o(\vec{r})$ and diffusion $\Phi_d(\vec{r})$ components of the fluence, respectively:

$$\Phi(\vec{r}) = \Phi_o(\vec{r}) + \Phi_d(\vec{r}) \qquad (2.19)$$

A similar relationship can be written for the direct $D_o(\vec{r})$ and the diffusion $D_d(\vec{r})$ components of the dose distributions:

$$D(\vec{r}) = D_o(\vec{r}) + D_d(\vec{r}) \qquad (2.20)$$

The total dose will be the superposition of doses generated by all partial sources. The relations between fluence and dose for the two components are:

$$D_o = W_o \Phi_o(\vec{r}) \quad \text{and:}$$

$$D_d = W_o R_o^d \Phi_d(\vec{r}) \qquad (2.21)$$

where W_o is the stopping power of a given material averaged over the partial spectrum considered, and R_o^d =const. is the ratio of stopping powers for the diffusion and directional components of the fluence.

For the directional component of the fluence the following expression can be written:

$$\phi_0(\vec{r}) = (4\pi r^2)^{-1} \exp[-\bar{\kappa}(\vec{r})r] \qquad (2.22)$$

where $\bar{\kappa}(\vec{r})$ is the mean value of the attenuation coefficient for the directional component, a constant in a homogeneous medium. For a heterogeneous combination, $\bar{\kappa}(\vec{r})$ is calculated as an average of the constant attenuation coefficients weighted by the path lengths of the different media lying between the source and the observation point.

In each medium "j" the diffusion component must satisfy the ordinary diffusion equation:

$$\Delta\phi_{dj} - \nu_j^2 \phi_{dj} = -\frac{Q\delta(r)}{4\pi r^2 D_j} \qquad (2.23)$$

corresponding to a point diffusion source located at r=0 with a strength Q. Here D_j and ν_j are the diffusion coefficient and the absorption coefficient respectively for the fluence in

the "j" medium, while $\delta(r)$ is the delta function. The equation (2.23) is solved separately for Φ_d in each medium and the constants appearing by integration are chosen so as to satisfy the boundary condition of continuity. The parameters ν, $\alpha=\kappa/\nu$, νD, Q, R_o^d are given empirically determined values.

For a planar geometry, as shown in Fig.3.1, by solving equations 2.22, 2.23 and using 1 and 2 indices to indicate the two media under investigation, the dose as a function of the distance from the source may be written as:

$$D_1 = \frac{\sigma W_{01}}{2}\left\{E_1(\alpha_1 \nu_1 r) + R_0^d\left[\frac{Q}{\nu_1 D_1}\exp(-\nu_1 r) + \frac{2B}{\sigma}\exp(\nu_1 r)\right]\right\} \qquad (2.24)$$

for $r<r_0$, and:

$$D_2 = \frac{\sigma W_{02}}{2}\left\{E_1[\alpha_1 \nu_1 r_0 + \alpha_2 \nu_2 (r - r_0)] + R_0^d \frac{2C}{\sigma}\exp(-\nu_2 r)\right\} \qquad (2.25)$$

for $r>r_0$.

Where r_0 is the distance from the source to the interface, Q=0.5, σ is the partial activity per unit area, A, B, and C are constants and $E_1(x)$ is given by:

$$E_1(x) = \int_x^\infty t^{-1}\exp[-t]dt \qquad (2.26)$$

The same method applied for a homogeneous medium (E.g. medium 1) yields the following expression for the dose distribution :

$$D_{h1} = \frac{\sigma W_{01}}{2}\left\{E_1\ \alpha_1 \nu_1 r\ + R_0^d \frac{Q}{\nu_1 D_1}\exp -\nu_1 r\right\} \qquad (2.27)$$

The difference between equations 2.24 and 2.27 then must represent the dose effect of the presence of the backscatterer (medium 2). For a fixed distance from source to backscatterer r_0, this can be written as:

$$D_{dif} = D_1 - D_{h1} = W_{01} B R_o^d \exp(-\nu_1 r) \qquad \text{or,}$$

$$D_{dif} = D_1 - D_{h1} = const \cdot \exp(-\nu_1 (r_0 - r)) \qquad (2.28)$$

changing the variable to $x = r_0 - r$, which represents the distance backwards from the interface, the expression now becomes:

$$D_{dif} = const \cdot \exp(-\nu_1 x) \qquad (2.29)$$

The backscatter coefficient $B_{1(r_0)}=D_{dif}/D_{h1}$ close to the interface ($r \rightarrow r_0$) can be expressed as:

$$B_1(r_0) = \frac{R_0^d \frac{2B}{\sigma}\exp(\nu_1 r_0)}{E_1(\alpha_1 \nu_1 r_0) + R_0^d \frac{Q}{\nu_1 D_1}\exp(-\nu_1 r_0)} \qquad (2.30)$$

which becomes a constant for large r_0 (saturation value) as the directional component E_1 becomes negligible compared to the diffusion component. The saturation value at zero distance from the interface simplifies to:

$$B_{sat}(r_0) = \frac{\nu_1 D_1 - \nu_2 D_2}{\nu_1 D_1 + \nu_2 D_2} \qquad (2.31)$$

According to the Two Group method predictions, the backscatter factor at the interface should reach a saturation value at a certain distance from the source to the interface r_0 and decrease with decreasing distance.

2.8. The Spline Approximation

The spline interpolation approximation is a widely used method of smoothing and interpolating discrete experimental data for further processing. Rather than using a single function to fit the entire data set , the fit is made with piecewise functions defined on individual portions of data set while satisfying certain conditions regarding the continuity of the function and its derivatives. It could be inferred that the method is suitable to any data pattern.

All data processing in the present work was done using a set of subroutines of spline polynomial representation, by Paul Dierckx, department of computer science, Leuven-Belgium. The subroutines used are SMOOT.F for the determination of the best spline fit for a given set of data, SPLEV.F for the evaluation of the spline fit at particular abscissa points, SPLDER.F for derivation of the spline representation and SPLINT.F for integration. These subroutines are part of the FITPACK (Dierckx) FORTRAN package for calculating smoothing splines for various kinds of data and geometries. The package is available on the internet at the address http://www.netlib.org/dierckx/.

Basically, given a set of data points (x(i), y(i)) and a set of correspondent positive numbers (weighting) w(i), i=1,2,....m, a spline polynomial function s(x), of degree k, made to pass through certain data points, which are called knots, is a function that has the following properties: in each interval between two knots, s(x) is given as a polynomial of degree k or less and, s(x) and its derivatives of order 1,2,.....(k-1) are continuous everywhere (Greville 1969). The number and the position t(j), j=1,2,....n of the knots is chosen automatically by the routine. The amount of smoothness is determined by the condition that:

$$\sum_i (w(i)\cdot(y(i)-s(x(i))))^2 \le s \qquad (2.32)$$

where s is a user supplied positive constant called the smoothing factor. As can be seen in the equation (2.32), setting s=0 forces the spline representation s(x) to cross all the initial discrete data. The weighting factor is usually taken as one over the standard deviation squared.

CHAPTER 3.

3. The Scaling Factor of Water to Bone

3.1 Method

This work investigates the particular case of potential practical interest of deriving beta-ray dose distributions in bone [compact bone ICRU (1964)] from those in water using the scaling method.

The most recent value of the scaling factor of water to bone available in the literature is η_w=0.973, given by Cross (1992), with an estimated accuracy of 1%. It should be mentioned that this value is arrived at via an indirect evaluation using the scaling factors relative to air. The reference medium air was converted to water using equation (2.18).

Thus far, the scaling factors have been calculated (Berger 1971) as the ratios of percentile distances in the two media. The percentile distance is defined as the radius of a sphere within which the absorbtion of a fixed percentage of the emitted energy of a point beta source has occurred. The average of the scaling factors calculated for different percentages (e.g. 10,30, 50, 70 and 90% used by Berger) is taken as the final result.

A statistical approach was used in the present work to calculate the scaling factor of water to bone. The shapes of the two dose distributions, in water and bone respectively, were examined in detail to ascertain if they are indeed related solely by a scaling factor and, to the extent that this is true, an optimum value for the factor was calculated.

3.2 Data collection and analysis

The data for depth-dose distributions were generated by running the TIGER code, version 2.1, on VAX-4400 and VAX-3100 machines.

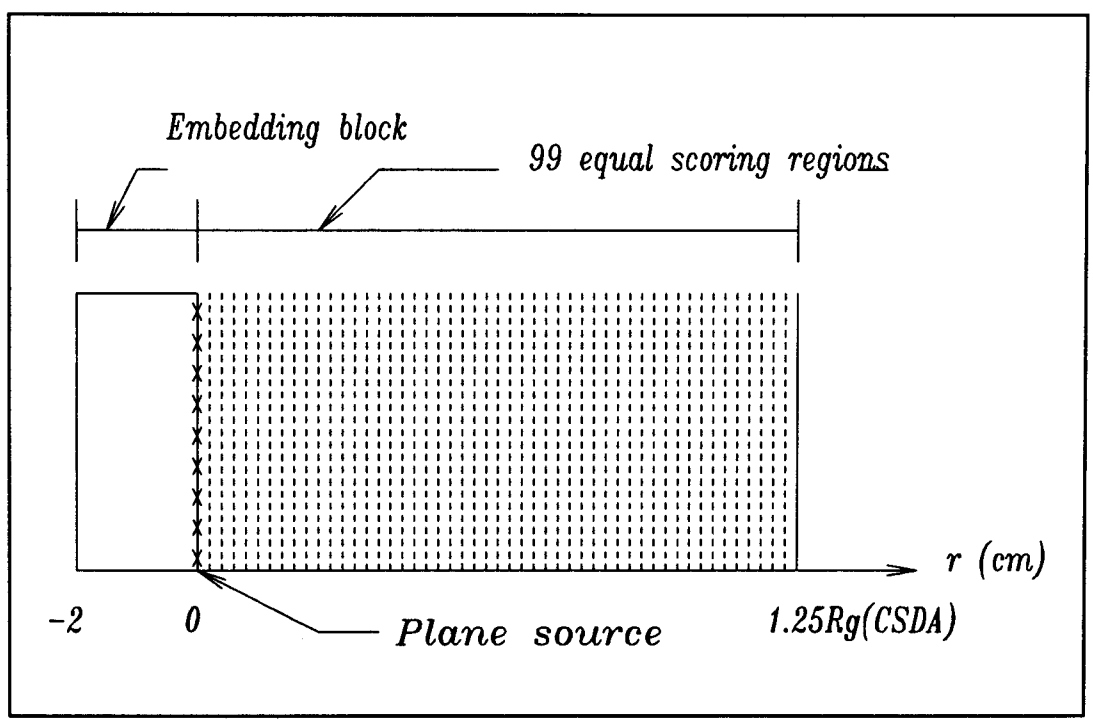

Fig.3.1. Plane geometry used in the Monte Carlo calculations.

Fig. 3.1 displays the planar geometry used for the calculations. Rather than the thin scoring regions used to obtain "point" values for the deposited energy, a sequence of contiguous scoring regions of a uniform depth was preferred. The geometry consists of an embedding block of 2 cm depth followed by 99 equal depth planar scoring region layers. In between the block and the scoring region an isotropic plane source of negligible thickness is located. The purpose of the 2cm block is to eliminate any interface effect on the dose deposition, the maximum electron range being less than 2 cm for all the energies investigated. The media used were thus homogeneous in either water or bone. The scoring regions extended to $1.25R_g$, where R_g is the CSDA (Continuous Slowing Down Approximation) range in the appropriate medium.

The TIGER code was run for planar isotropic monoenergetic beta sources at the energies of 0.1, 0.5, 1.0, 1.5 and 2.0 MeV, energies which cover the majority of the radioisotope beta spectra.

Each run consisted of 200 000 histories distributed uniformly over ten batches. Computing time required for the simulations varies with the source energy, longer time being needed for higher energies. In general, run times were between 5 and 10 cpu hours. The contribution of secondary photons, bremsstrahlung photons and relaxation radiation was neglected, being insignificant for the energies considered. For the highest electron energy investigated, 2 MeV in water, the dose contribution of the secondary photons is about 1% at a distance of $0.81 g/cm^2$, a distance within which 99.75% of the initial beta energy is deposited and much lower at shorter distances. The cutoff energy parameter in

the Monte Carlo run for electrons was taken to be 9 keV, according to the method given in Halbleib (1984). At this energy the electron history was terminated and on-the-spot energy deposition occurred.

The dose relative statistical uncertainties in the TIGER code output were 0.5 to 2% for the depth within which 99% of the energy is deposited, and increased up to 10% at the range limits. Table 3.1 summarizes the physical properties of the two media considered.

Table 3.1. Physical properties and chemical compositions of water and bone (compact ICRU).

	Density ρ(g/cm^3)	<Z/A>	Effective atomic No. $\overline{Z}$	Chemical composition constituent : fraction by weight
Water	1.00	0.555	8.743	$_1$H:0.111894 $_8$O:0.888106
Bone ICRU	1.85	0.530	6.599	$_1$H:0.063984 $_6$C:0.278000 $_7$N:0.027000 $_8$O:0.410016 $_{12}$Mg:0.002000 $_{15}$P:0.070000 $_{16}$S:0.002000 $_{20}$Ca:0.209930

The averaged ratio of the atomic number to the atomic mass <Z/A> and the effective atomic number $\overline{Z}$ are calculated with the expressions (3.1) (Beger 1982) and (3.2) (Cross 1968), respectively:

$$\left\langle \frac{Z}{A} \right\rangle = \sum_{i=1}^{n} p_i \frac{Z_i}{M_{Ai}} \qquad (3.1)$$

$$\overline{Z} = \frac{\sum_{i=1}^{n} p_i \frac{Z_i^2}{M_{Ai}}}{\sum_{i=1}^{n} p_i \frac{Z_i}{M_{Ai}}} \qquad (3.2)$$

where Z_i is the atomic number of the constituent element i, p_i is the fraction by weight of the element i, M_{Ai} is the atomic mass of the element i, and n is the total number of elements in the medium.

A program was written to compare the depth dose distribution curves in both media using a generalized chi-squared test. The best fit on 100% CSDA-range in bone was found for each energy investigated by minimizing the value of χ^2 with the variation of the scaling factor η_w . The χ^2 is given by:

$$\chi^2 = \sum_i \frac{\left[\eta_w I_w(\eta_w z_i) - I_b(z_i)\right]^2}{\sigma_{wsi}^2 + \sigma_{bi}^2} \qquad (3.3)$$

where σ_{wsi}, σ_{bi} are the statistical errors in dose deposition determined for water scaled to bone and bone respectively, $I_w(z_i)$ and $I_b(z_i)$ are the dose deposition curves in water and bone respectively versus the depth z (z_i in g/cm^2) and η_w is the scaling factor of water relative to bone. The scaling to bone was done according to the relationship (2.15).

The χ^2 variation with the "parameter" scaling factor η_w was evaluated using an increment of 10^{-4}. Then, the χ^2 data were fitted with a parabola, the vertex of which gives the least-squared value for the scaling factor. The variation in relative attenuation that generates an increase of one in the value of χ^2 is a measure of the scaling factor standard deviation (Bevington 1992).

The data processing for the generalized chi-squared test was done by using a five degree polynomial spline interpolation with a zero smoothing factor.

Table 3.2 summarizes the results of the χ^2 analysis and a plot of the data is shown in Fig. 3.2. The scaling factor values obtained differ from each other by less than 0.2% for the five energies investigated. The average scaling factor found is consistent with Cross's value (0.973 ± 0.009) but represents an order of magnitude increase in accuracy.

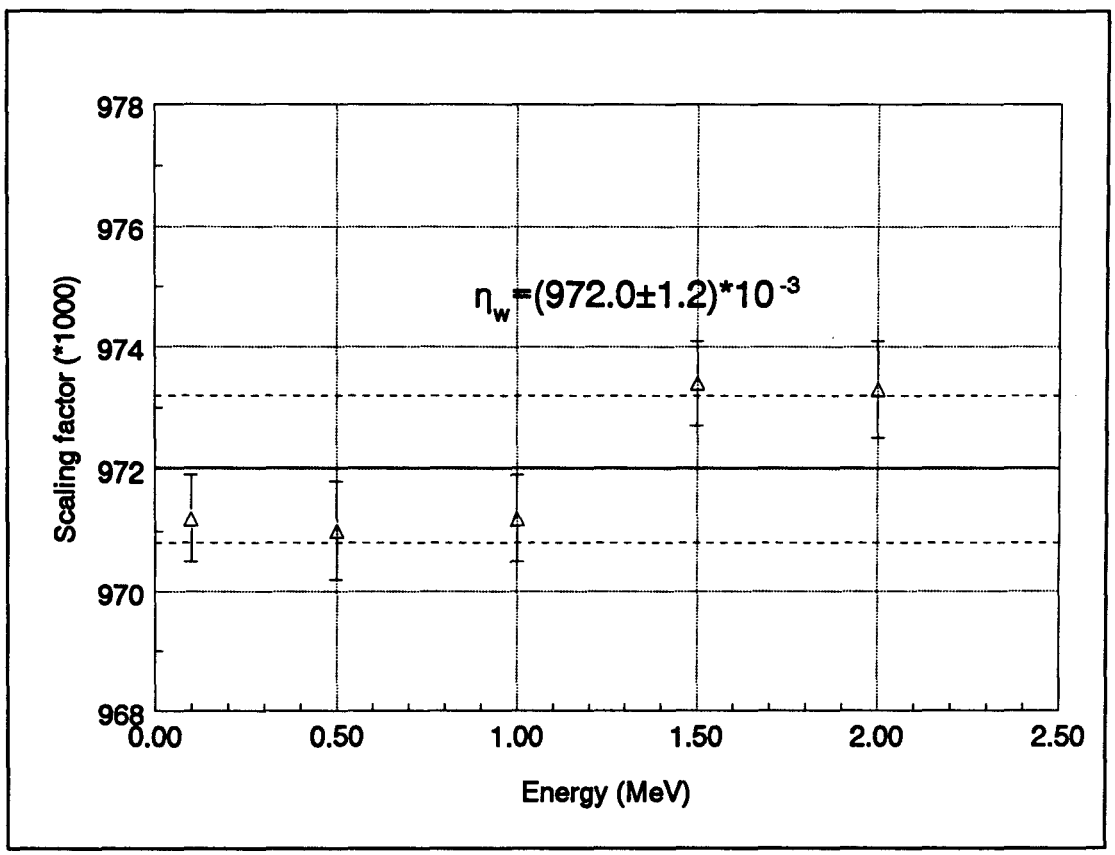

Fig. 3.2 Scaling factors water to bone (compact-ICRU) for monoenergetic electrons in the energy range 0.1 to2.0 MeV.

Table 3.2. Scaling factors water to bone for monoenergetic electrons 0.1-2.0 MeV.

E(MeV)	η_w 10^{-3}	σ
0.1	971.2	0.7
0.5	971.0	0.8
1.0	971.2	0.7
1.5	973.4	0.7
2.0	973.3	0.8

Average scaling factor:
$\eta_w=(972.0\pm1.2)\ 10^{-3}$

The ratio of the dose in bone over the dose in water scaled to bone versus the dimensionless depth (depth over range in bone for the specific energy x=z/Rb) was investigated as the most sensitive way to compare the accuracy of the scaling method.

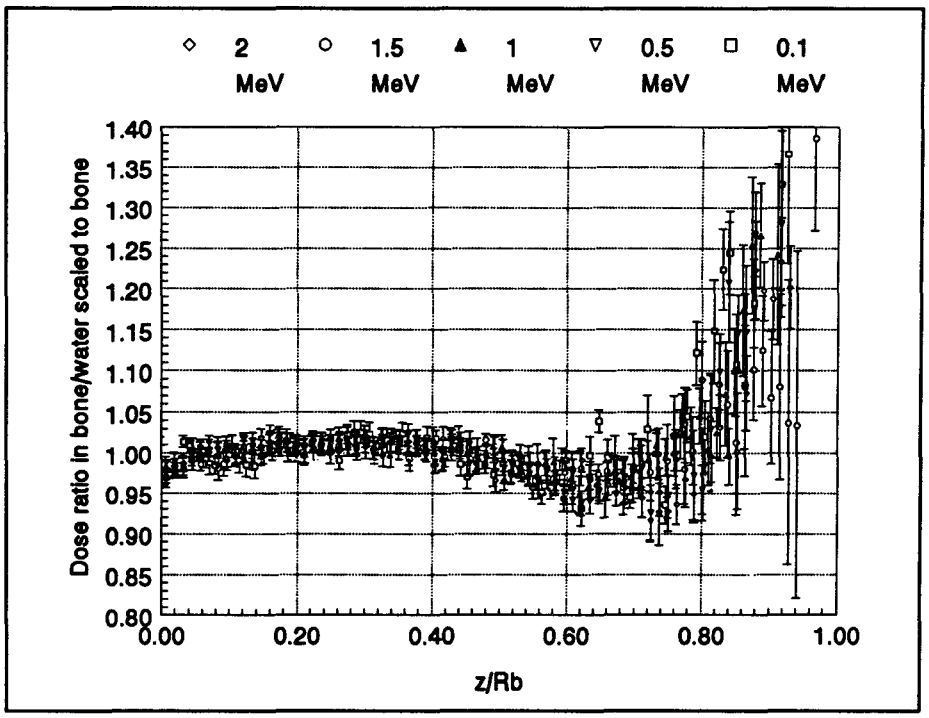

Fig. 3.3 The ratio of dose in bone over dose in water scaled to bone for monoenergetic electrons in the energy range 0.1 to 2.0 MeV.

After scaling the water curve to bone with the average factor 0.9720 the agreement with the dose deposition curve in bone is within 5% difference for the depth extending to 60% of the range, corresponding to the depth within which 95% of total energy is deposited (Fig. 3.3).

Moreover, the same trend with dimensionless depth was observed for the ratio of dose in bone to that in water-scaled to bone for all energies. Fig. 3.4 shows this trend where the data were averaged in sets of five.

The accuracy of the scaling method for monoenergetic dose kernels may be improved by defining the "modulation function", F(x), as:

$$F(x) = \frac{I_B(x)}{\eta_w \cdot I_w(\eta_w \cdot x)} \qquad (3.4)$$

The derivation of the dose distributions in bone from those in water can be achived with scaling and modulation, according to the relationship:

$$I_B(x) = \eta_w \cdot I_w(\eta_w x) \cdot F(x) \qquad (3.5)$$

where $I_B(x)$ is the depth dose deposition in bone, $I_w(x)$ is the depth dose deposition in water and x is the dimensionsless depth z/range in bone for the specific energy.

Fig. 3.4. displays the modulation function in a six degree order polynomial representation obtained by fitting the observed trend in the ratio of dose in bone to that in water scaled to bone, data averaged in sets of five.

The ratio of the dose in bone to that in water scaled and modulated to bone (equation 3.3) is illustrated in Fig.3.5. By using the modulation function F(x), agreement

whithin 3% was achieved between observed dose in bone and dose in water scaled and modulated to bone for up to 80% of the range, equivalent to a depth within which 99% of the energy is deposited. The correction provided by the modulation function is about 3% for regions close to zero, up to 1% for x between 0.1 and 0.45, up to 4% for x between 0.45 and 0.80 and, higher for the rest of the track.

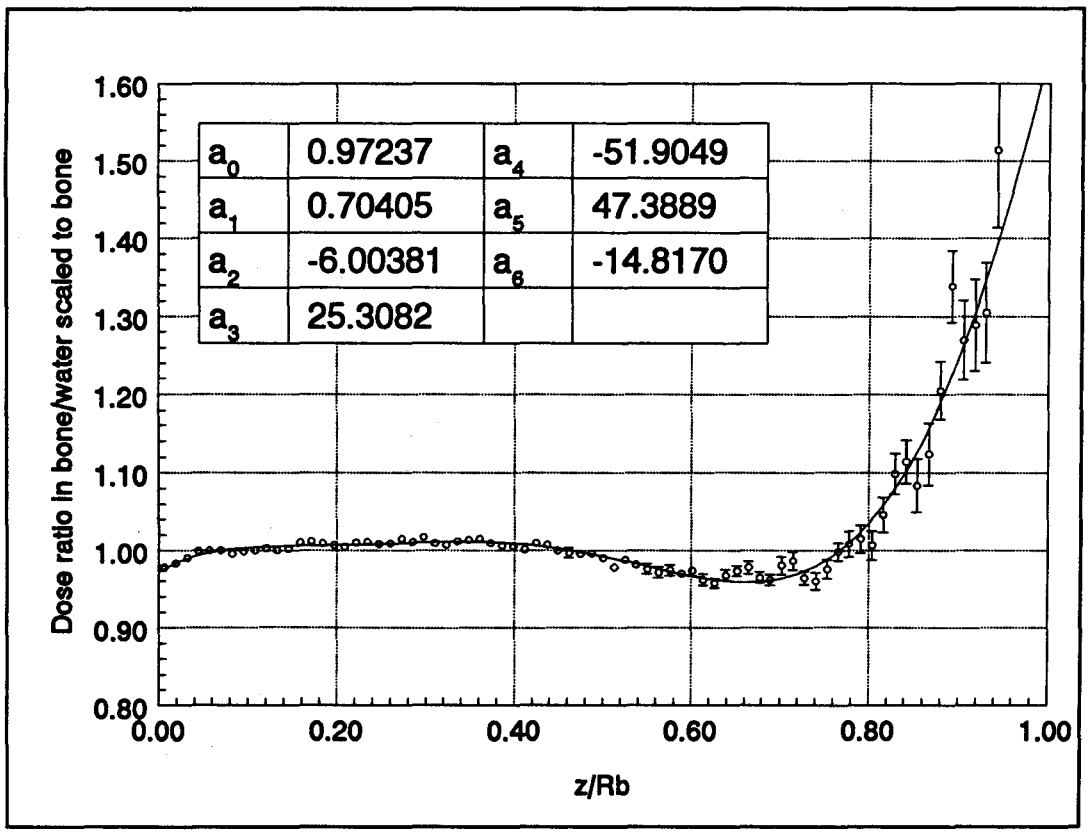

Fig. 3.4. Modulation function F(x) in a six degree polynomial representation in plane geometry (—— continuous line) and the ratio dose in bone to that in water scaled to bone. Data averaged in sets of five (o marker).

The amount of the average energy deposited in water as a function of depth in percentage of range is given in the Table 3.3.

Table 3.3. Energy deposited in water by beta particles versus depth, in percentages.

Energy (% of total)	50%	80%	85%	90%	95%	99%
Depth (% range)	20%	42%	46%	53%	63%	77%

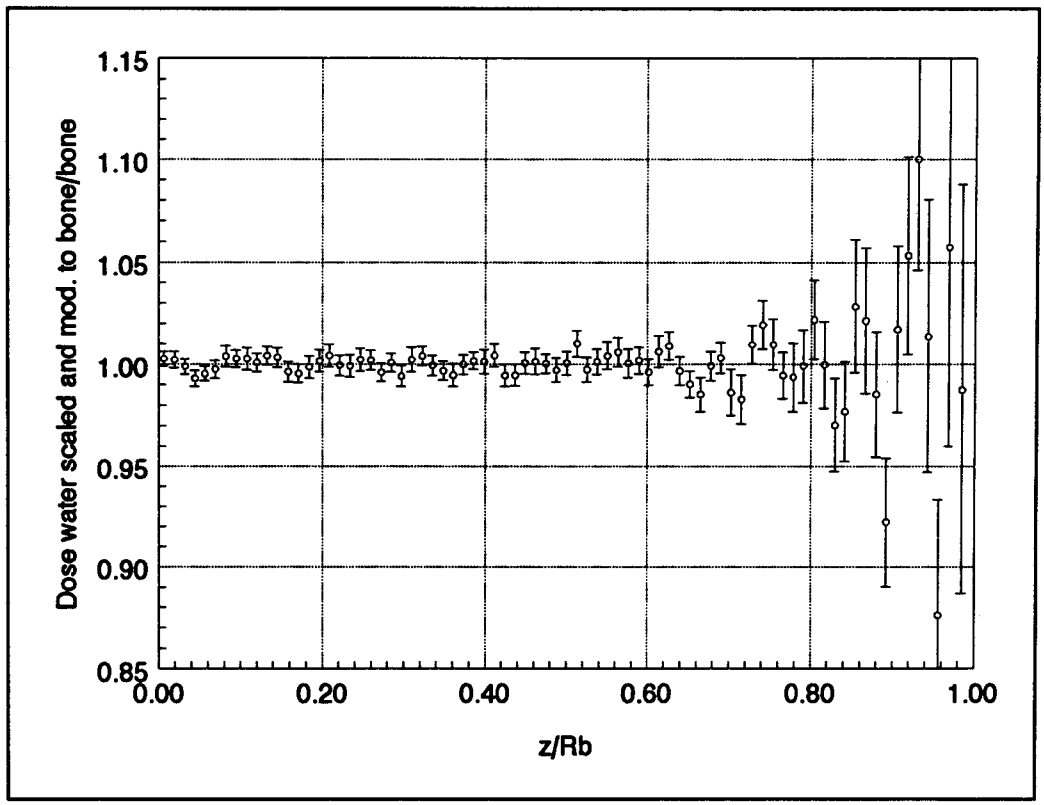

Fig. 3.5. Ratio of dose in water scaled and modulated to bone to that in bone for electrons of 0.1-2.0 MeV energy. Data averaged in sets of five.

3.3 Modulation function for the point geometry

The form of the modulation function was investigated for switching from plane to point geometry. Data for dose deposition in point geometry J(r) were derived from those in plane geometry I(z) according to the equation (Loevinger 1954) :

$$J(r) = \frac{1}{2\pi \cdot z} \cdot \left(-\frac{dI}{dz} \right) \qquad (3.6)$$

The accuracy of deriving depth-dose distributions from plane to point geometry was checked by comparing the results with Cross's data (Cross 1992) where available, namely for water at 0.1, 1.0 and 2.0 MeV electron energies (Fig. 3.6). Cross's calculations were done using the ACCEPT-P Monte Carlo code designed for point geometry. The derived point depth-dose distributions and data comparison was done in terms of the dimensionless quantity $j(r/r_E,E)$. Rather than the dose deposition versus depth r, the quantity $j(r/r_E,E)$ is the preferred representation for a point isotropic source in a infinite medium and it is defined as:

$$j(r/r_E,E)=4\pi\rho \cdot r^2 \cdot J(r) \cdot r_E/E \qquad (3.7)$$

where r (cm) is the distance from the source, r_E (cm) is the nominal CSDA range, E (MeV) is the electron energy and ρ (g/cm^3) is the density of the medium.

The use of the quantity $j(r/r_E,E)$ instead of the dose J(r), combined with a smoothing procedure of averaging in sets of eleven data, eliminated problems arising from

high sensitivity to statistical fluctuations encountered when deriving dose distribution from plane geometry using equation (3.6). Except at very short distances the dose in water derived from plane geometry is generally within 3% of Cross's data. A similar agreement within 3%, and higher differences for very short distances, was reported by Cross (1992) comparing the results of two Monte Carlo codes ACCEPT and ETRAN. No reason for the poor fit at short distances is known.

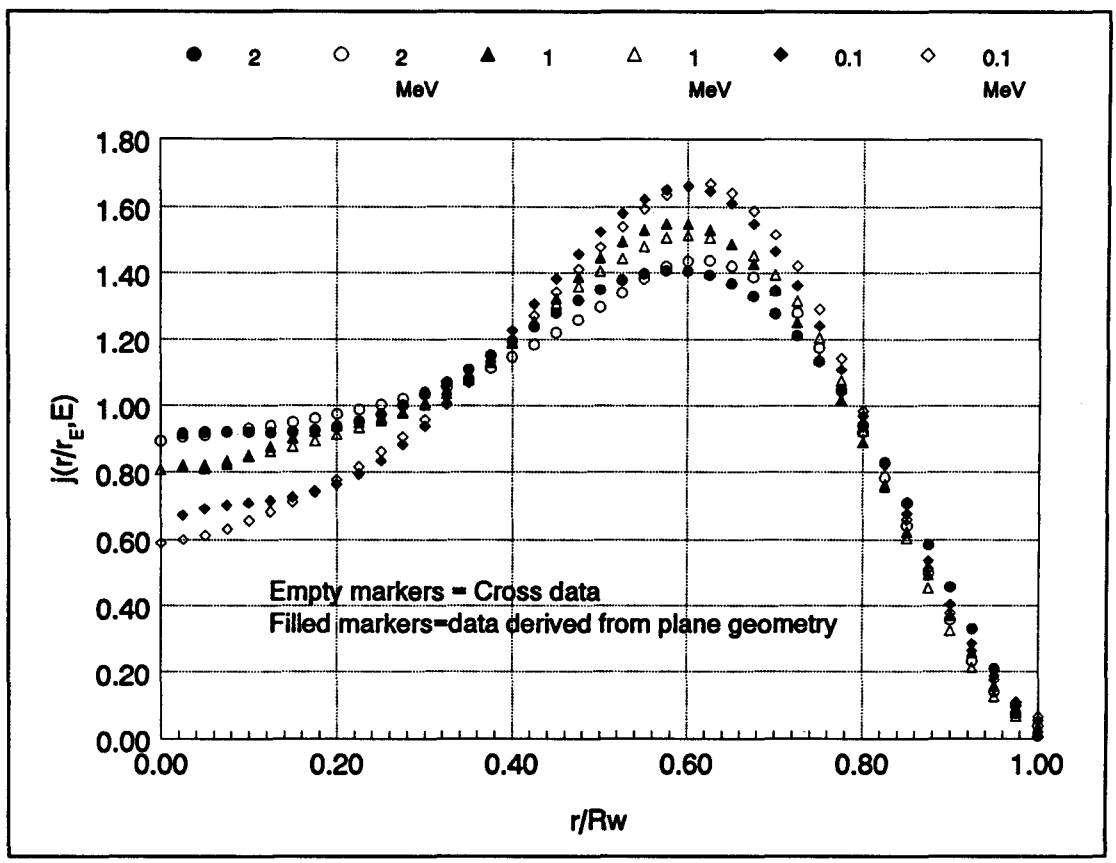

Fig. 3.6. Depth dose distribution in water for point geometry derived from plane geometry (filled markers) compared to Cross' s data (empty markers), directly calculated in point geometry.

The modulation function for the point geometry, M(x), was derived relative to the modulation function in plane geometry F(x). This method was more preferable than the direct determination, as used in plane geometry, because the derivative of $\ln(I_S)$ is less sensitive to the statistical fluctuations than the derivative of I_S. Thus, the ratio dose in bone $J_B(r)$ to that in water scaled to bone $J_S(r)$ was considered, where the two quantities were calculated as:

$$J_B(r) = \frac{1}{2\pi \cdot z} \cdot \left(-\frac{d\left(F(z) \cdot I_S\right)}{dz} \right) \qquad (3.8)$$

$$J_S(r) = \frac{1}{2\pi \cdot z} \cdot \left(-\frac{dI_S}{dz} \right) \qquad (3.9)$$

so that :

$$M(x) = \frac{J_B(x)}{J_S(x)} = F(x) + \frac{1}{R_{gb}} \cdot \frac{dF(x)}{dx} \cdot \frac{d}{dz}\left(\ln I_S\right) \qquad (3.10)$$

where $x=z/R_{gb}$ is the dimensionless depth over the specific range in bone R_{gb} and $I_S(z)=\eta_w \cdot I_w(\eta_w z)\cdot$dose in water scaled to bone in plane geometry.

The transformation through scaling and modulation in point geometry may by written now as:

$$J_B(x) = \eta_W^3 \left(\frac{\rho}{\rho_W} \right)^2 \cdot J_W\left(\eta_W \cdot x\right) \cdot M(x) \qquad (3.11)$$

The data calculated were also fitted with a six degree polynomial for all the energies investigated. Fig.3.7. shows the results of calculations for all energies investigated and the fitting polynomial.

The modulation function for the point geometry provides a correction up to 8% for depths between 0 and 85% of the range in bone, and higher effect for further into the medium.

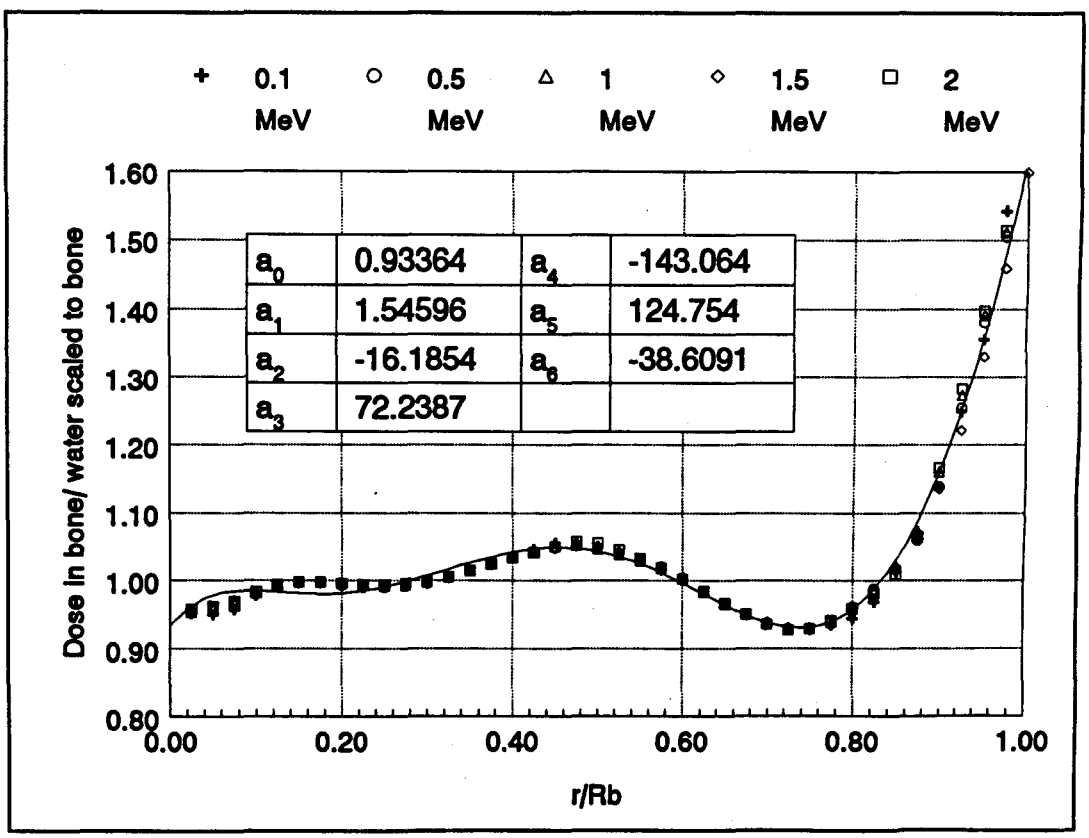

Fig. 3.7. Modulation function for point geometry M(x) in a six degree polynomial representation.

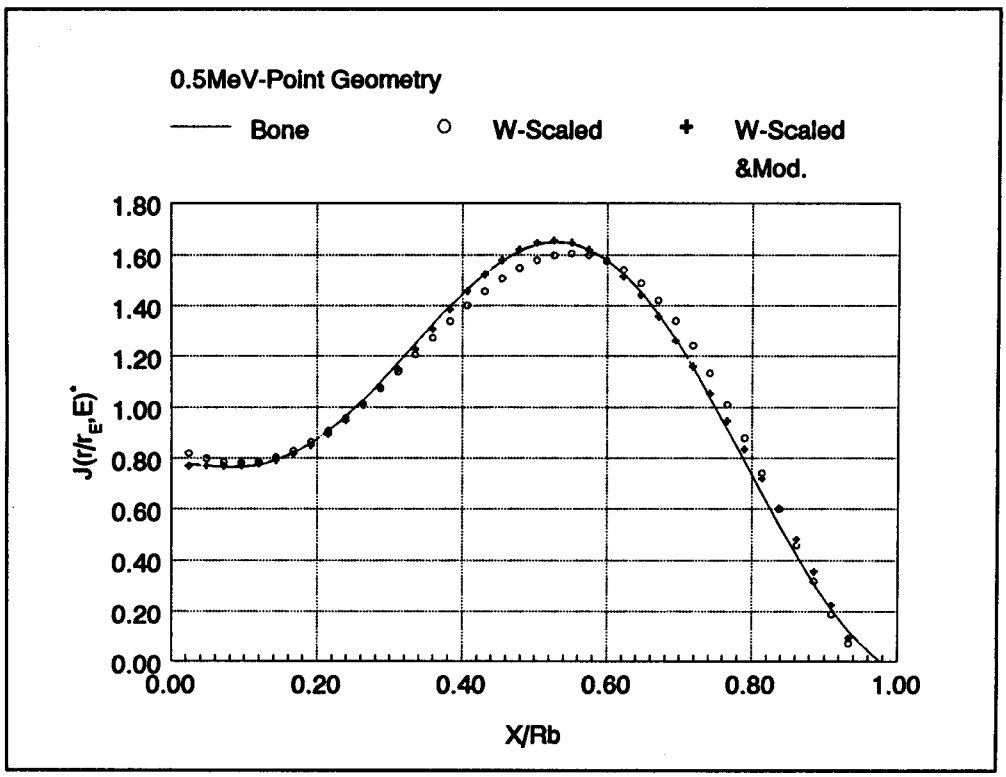

Fig. 3.8. Depth-dose distribution for 0.5 MeV monoenergetic electrons in point geometry: bone ICRU (— continuous line), water scaled (o marker), water scaled and modulated (+ marker)

Fig 3.8 compares graphically the dose distribution deposited by 0.5 MeV monoenergetic electrons in bone, in water simply scaled and in water scaled and modulated to bone. The improvement by using the modulation function M(x) is obvious even though the dose deposition data in the point geometry were affected by error propagation through calculation and differentiation.

3.4 Comments

By using a generalized chi-squared test, a detailed shape examination of the depth-dose deposition curves was conducted to determine the accuracy of the scaling method. A scaling factor of water to bone, η_w=(972.0±1.2) 10^{-3}, was determined. This new value is consistent with the one cited in literature, being within the uncertainties, but the accuracy of the determination proved to be almost an order of magnitude higher.

A universal modulation function was defined, which can improve the method of scaling for deriving the monoenergetic dose kernels in bone from those in water. The transformations by scaling and modulation are given by the relationships (3.5) or (3.11) in plane and point geometry, respectively. The modulation functions were determined as six degree polynomial representations for both geometries, plane F(x) and point M(x), for a dimensionless depth relative to the range in bone.

In terms of the accuracy of the scaling method, the modulation functions are graphical representations of the difference between the dose in bone and the approximate dose in bone derived from water using the scaling method for electron energies up to 2 MeV, energies which cover the most of the beta radioisotopes' spectra. The error of the method for the two similar atomic number media, water and bone-ICRU, is within 5% up to at least 60% of the range in bone, a depth within which 95% of the initial energy is deposited (Fig. 3.4 and Fig. 3.7). For depths larger than 80% of the range, the dose is

underestimated by this method. At the very beginning of the electron track the dose is overestimated with 2% in plane geometry and with about 5% in point geometry.

For the plane geometry, close to the source where the initial incident electron energy is not altered, it can be assumed that the energy deposited is roughly directly proportional to the ratio of the atomic number to atomic mass <Z/A>, as the most predominant term in the stopping power expression (2.4). This ratio <Z/A> is 5% higher for water than for bone (Table 3.1). The scaling factor makes a correction of 3% (η_w=0.972), thus, the resulting 2% discrepancy is expected. For the point geometry, however, a similar approximation cannot be made due to the rapid variation of the dose J(r) with the depth ($\propto 1/r^2$).

CHAPTER 4.

4 Scaling Factor Method for Dissimilar Media, Planar Interface

4.1 Method and Geometry

The scaling factor method of derivation of beta-ray depth dose distributions from one medium taken as the reference medium to another, in particular the derivation of beta-ray dose distributions in other media from those in water, was used only for the case of an homogeneous medium. This work is an attempt to enlarge the applicability of the above mentioned method to the case of dissimilar media, in its first step, a planar interface.

The method of investigation was to compare the accurate Monte-Carlo calculations with the results of scaling applied as described below. Fig.4.1 displays the geometry used for calculations. It consists of a thin isotropic planar source embedded to a depth r_o into medium 1, designated as the base. Medium 2, of higher atomic number Z in our experiment, is designated as the scatterer. The source to interface distance r_o is lower than the maximum electron range. Both the medium 1 slab behind the source and the

medium 2 slab are large enough to provide total attenuation of the electrons. The source and the interface of the two adjacent half media are parallel.

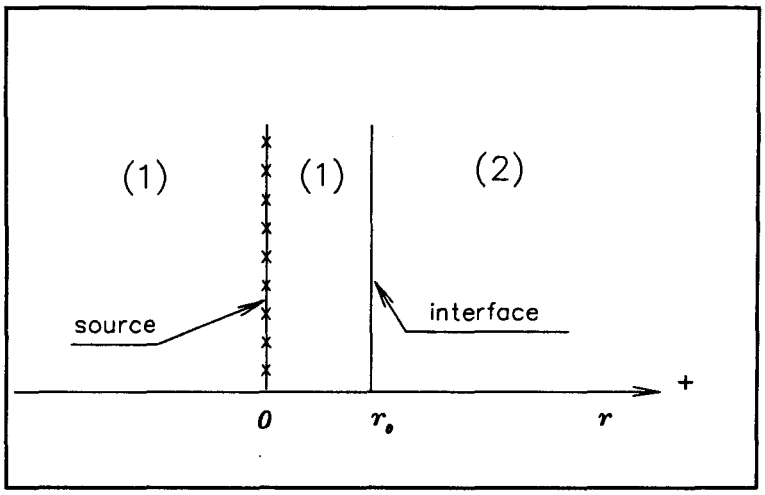

Figure 4.1. Geometry of Monte Carlo calculations(r in g/cm^2)

Water was always used as the base in our calculations. Water is a preferred approximation for tissue in the Monte Carlo calculations because it has a well defined chemical composition and its dose attenuation coefficient per g/cm^2 differs by less than 2% from those of various soft tissues, as defined by ICRP 1975 (Cross 1992).

Different from the homogeneous case is the presence of the dose backscattering effect due to the interface. We assumed that it is possible to derive the dose deposition I(r) for a planar interface (water-medium "i") from the dose deposition in homogeneous water $I_w(r)$. This may be done by reshaping the dose deposition curve from water to medium "i" in the backscatterer with the help of the scaling method and by correcting both doses, in the base and in the backscatterer, for the backscattering effect.

Mathematically the approach can be written as:

$$I(r)=\begin{cases} I_w(r)+F_B(r) & r < r_0 \\ \eta_w \cdot I_w \cdot [\eta_w \cdot (r-r_0)+r_0] \cdot n_B & r > r_0 \end{cases} \qquad (4.1)$$

where r is the distance from the source , r_0 is the source to interface distance (in g/cm^2), η_w is the scaling factor of medium "i" relative to water and, $F_B(r)$ and n_B are the necessary corrections due to the dose backscattering effect for base and backscatterer respectively.

4.2 Data collection

The PC-version of the same Tiger-Monte Carlo code, version 2.1, was used for the depth-dose deposition data generations. All the runs were done on a Packard-Bell computer equipped with a 100MHz pentium microprocessor. Ninety-nine scoring zones of equal width of $100mg/cm^2$ or less were used for dose deposition monitoring. Relevant parameters for the Monte-Carlo runs are presented in Table 4.1.

The pure beta emitter P-32 was chosen for the source, as a radioisotope with potential applicability in radiotherapy. A program provided by Dr. W. Prestwich was used to generate the continuous allowed beta spectrum of the P-32. The algorithm for the beta

spectra calculations used in the program is given in (Prestwich 1989). According to the Tiger code input requirements the P-32 beta spectrum was quantified in seventeen energy bins, each of about 100keV width, (Fig.4.2). The numerical details of quantification are summarized in Appendix 4.1. Seventeen bins was considered sufficient to provide enough accuracy for the Monte Carlo runs since the average beta emitted energy calculated after quantification differed from the value given in (Lederer 1978) and from the value calculated with the continuous spectrum by less than 0.1%.

Table 4.1. Tiger Code: histories' number and the typical necessary running time.

Material	Scoring-zone width (μm)	Scoring-zone width (mg/cm^2)	Histories No.	Typical cpu time (hours)
Water	100	10.0	$2*10^6$	6.0
Bone-ICRU	40	7.40	$2*10^6$	6.0
Aluminum-Al	30	8.07	$1*10^6$	3.5
Calcium-Ca	50	7.75	$1*10^6$	3.25
Copper-Cu	10	8.93	$5*10^5$	1.75
Cadmium-Cd	10	8.65	$5*10^5$	1.75

A test run was completed for the homogeneous case of water and the resulting data were compared with data published by Cross. The quantified spectrum was also tested on two machines of different random number generators: a VAX-4400 and a PC-pentium machine. Cross's data are given without uncertainties (Cross 1992). Fig. 4.3 shows very good agreement among the three sets of data ,the differences are within the uncertainties. The largest differences occur near the end of the range where Cross also is

assuming higher uncertainties for his data, up to 2-3%. It should be mentioned that Cross's data were obtained by the integration of monoenergetic dose kernels over the P-32 spectrum in point geometry. The planar geometry data were subsequently derived by integration over an infinite plane source as given by the equation (2.12).

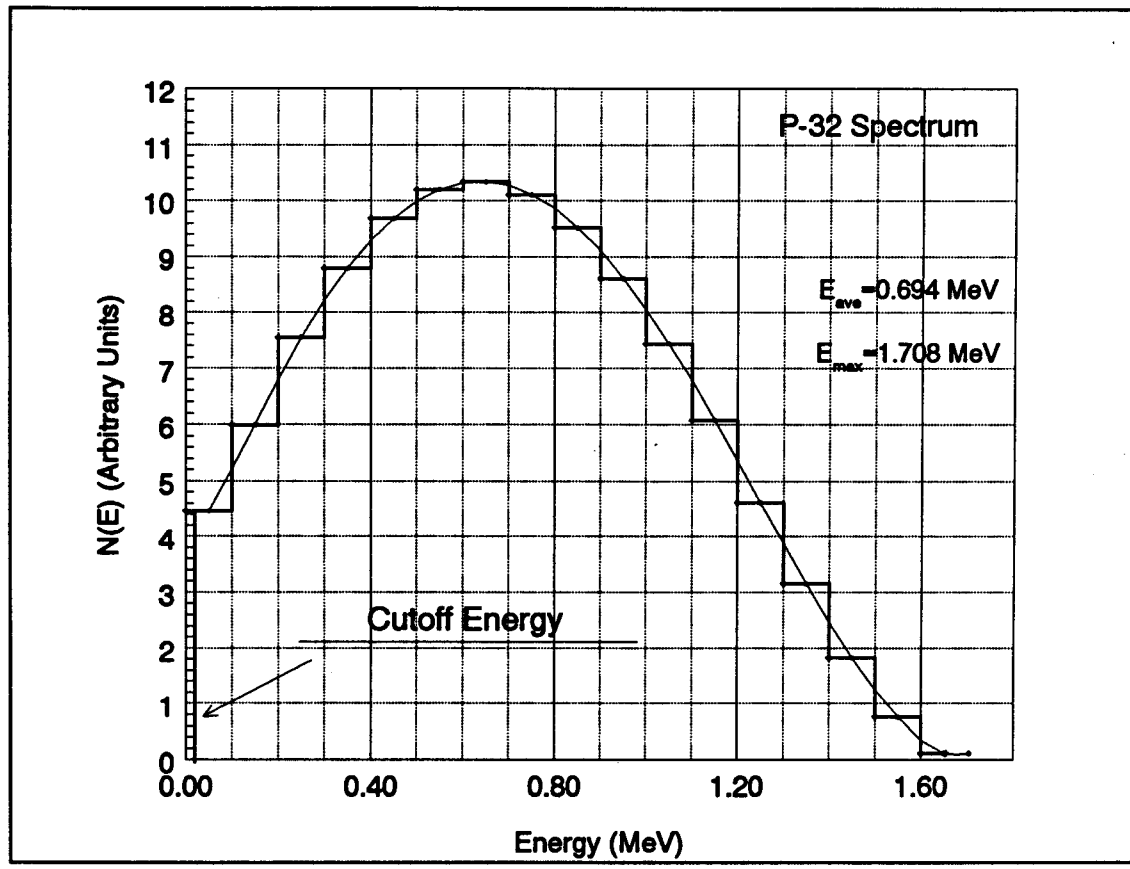

Fig.4.2 The quantification of the P-32 beta spectrum.

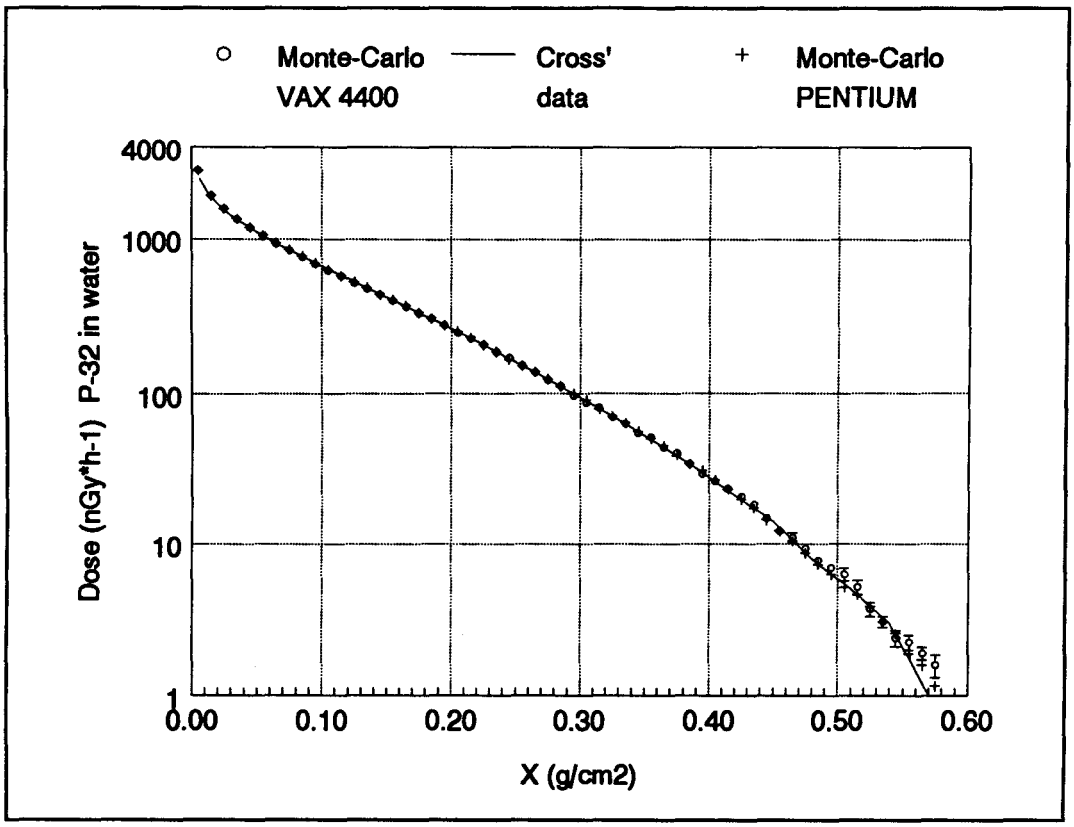

Fig. 4.3. Depth dose deposition in water :Cross's data (continuous line ——) compared to data obtained with the P-32 quantified spectrum on Vax-4400 (marker o) and on PC-pentium machine (marker +).

Table 4.2. Physical data for base and scatterres

Material	Effective atomic number $\overline{Z}$	Density (g/cm^3)	Chemical. Atomic Mass. u.m.	Scaling factor
Water	6.60	1.00	—	1
Bone-ICRU	8.74	1.85	—	0.972
Aluminum	13	2.69	29.98	0.893
Calcium	20	1.55	40.08	1.005
Copper	29	8.93	63.54	1.030
Cadmium	48	8.65	112.41	1.169

Table 4.2 summarizes the materials used as scatterers and their physical characteristics. The effective atomic number $\overline{Z}$ is calculated using the expression (3.2) (Cross 1968). Scaling factors relative to water were calculated using relationships (4.2) and (4.3) (Cross 1982, 1992).

The scaling factor relative to water is calculated as:

$$\eta_W = \begin{cases} 0.77\cdot(1+0.0491\cdot\overline{Z}-0.0009\cdot\overline{Z}^2)\cdot S/S_W & \overline{Z}<18 \quad \text{(Cross '92)} \quad (4.2) \\ 0.8254\cdot(1+0.0284\cdot\overline{Z})\cdot S/S_W & \overline{Z}\geq 18 \quad \text{(Cross '82)} \quad (4.3) \end{cases}$$

where S/S_W is the stopping power of the medium "i" relative to water. For Z>40 the slope of the curve (4.3) was decreased by 2%, as recommended by Cross for a better fit.

The relative stopping power varies somewhat with the energy. The ratio of the ranges of 500KeV electrons (r_{water}/r_{medium}) is taken arbitrarily as an average stopping power of the medium relative to water (Cross 1968). Ranges for various media are given in Berger (1982). In media for which ranges are not available two empirical expressions (4.4 and 4.5) can be used to calculate the relative stopping powers (based on the work of Roesch, 1954):

$$S/S_W = \begin{cases} 2.106\cdot\Sigma[W_iZ_i/A_i\cdot(1-\ln Z_i/11.5)] & \overline{Z}<18 \quad (4.5) \\ 2.0228\cdot\Sigma[W_iZ_i/A_i\cdot(1-\ln Z_i/13)] & \overline{Z}\geq 18 \quad (4.6) \end{cases}$$

The relationships (4.3) and (4.6) are derived from (Cross 1982) by changing the reference medium from aluminum to water.The assumed uncertainty of the scaling factor calculation is about 1-2% at low atomic numbers and up to 5% for Z=82.

Eight different positions (r_o) of the interface relative to the source were considered ranging from 50mg/cm^2 to 400mg/cm^2 in increments of 50mg/cm^2. The minimum at r_0=50mg/cm^2 was imposed by the necesity of having at least five values for a data fit interpolation. The upper limit, r_0=400mg/cm^2, was taken because in water at this depth about 99% of the initial energy is already deposited.

The number of electron histories in the Monte Carlo runs was increased for low atomic number materials (Table 4.1). The arbitrary rule followed was to have a large enough number of histories to provide uncertainties under 1% for approximately the first one third of the significant dose data. This rule gives a good balance between data accuracy and the running time.

The influence of the electron "Cutoffs" energy input instruction in the Tiger Carlo code was also investigated. Double sets of runs were done with 1keV and 9keV electron energy cutoffs, respectively. The cutoff energy instruction fixes the value of electron energy under which the electron history is terminated and on-the -spot deposition of the remaining energy is assumed.

4.3 Data analysis

A typical plot of the depth dose deposition with a water-cadmium interface situated at r_0=100mg/cm^2 compared to the depth dose deposition in a homogeneous medium of water is shown in the Fig. 4.4. Cadmium will be used as an illustrative example because the backscattering effect is more observable due to its relatively high atomic number (Z=48). Due to the backscattering effect more energy is deposited in the base in the dissimilar media case compared to the homogeneous situation. Subsequently, lower energy deposition occurs in the backscatterer.

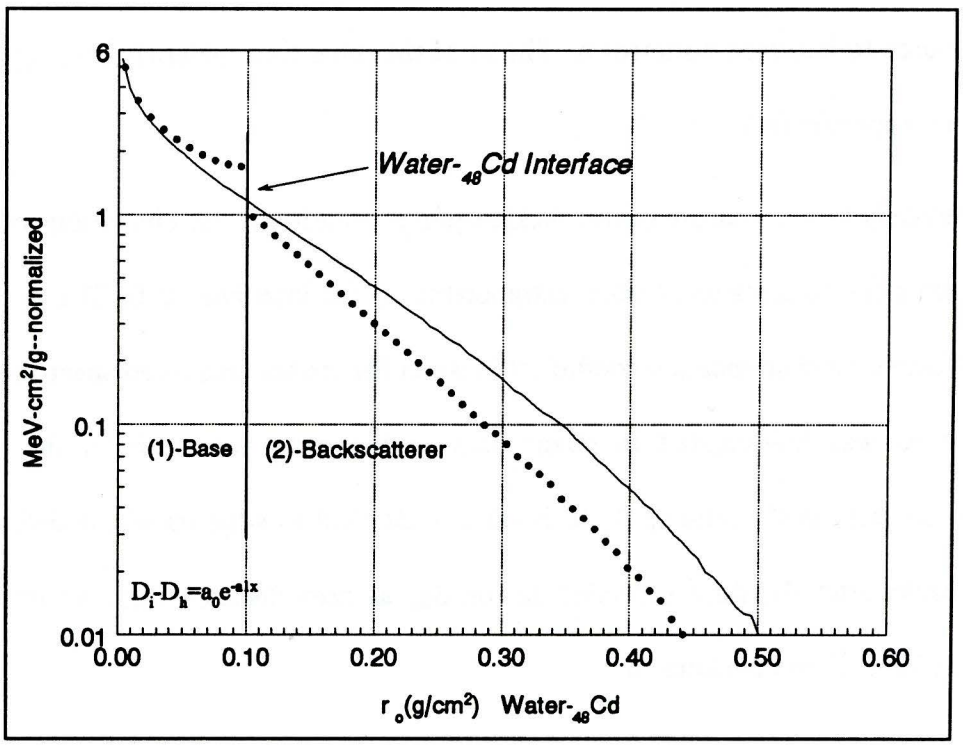

Fig.4.4 Dose depth deposition for a water-$_{48}$Cd interface (marker o) and for homogeneous water (continuous line —). P-32 planar source at zero coordinate.

4.3.1 Depth Dose Deposition in Base

Let $D_h(x)$ be the dose in the homogeneous case and, $D_i(x)$ be the dose for a geometry with an interface, $x=(r_0-r)$ being the distance from the interface backward to the source in g/cm^2. A very good fit of the difference $F_B(r)\equiv D_d(x)=D_i(x)-D_h(x)$ has been found with an exponential function of the type:

$$D_d(x) = a_0 \cdot e^{-a_1 \cdot x} \qquad (4.7)$$

Fig. 4.5 shows the fitting of the dose difference $D_d(x)$ for a water-$_{48}$Cd interface for different source to interface distances r_0. The fit of the other four materials investigated is presented in Appendix (4.2).

Physically a_0 is a measure of the backscattering intensity. It has dimensions of dose and represents the backscattered dose extrapolated to the interface, x=0. The a_1 is an average effective mass attenuation coefficient in water for the backscattered spectrum.

The a_0 was investigated in relationship to the dose deposition in the water homogeneous case, as the ratio a_0/D_h. This ratio is identical to what usually is defined as the dose backscatter or, dose reflection factor B_{ih}, at zero distance from an interface between medium "i" and medium "h":

$$B_{ih} = \frac{D_i}{D_h} - 1 \qquad (4.8)$$

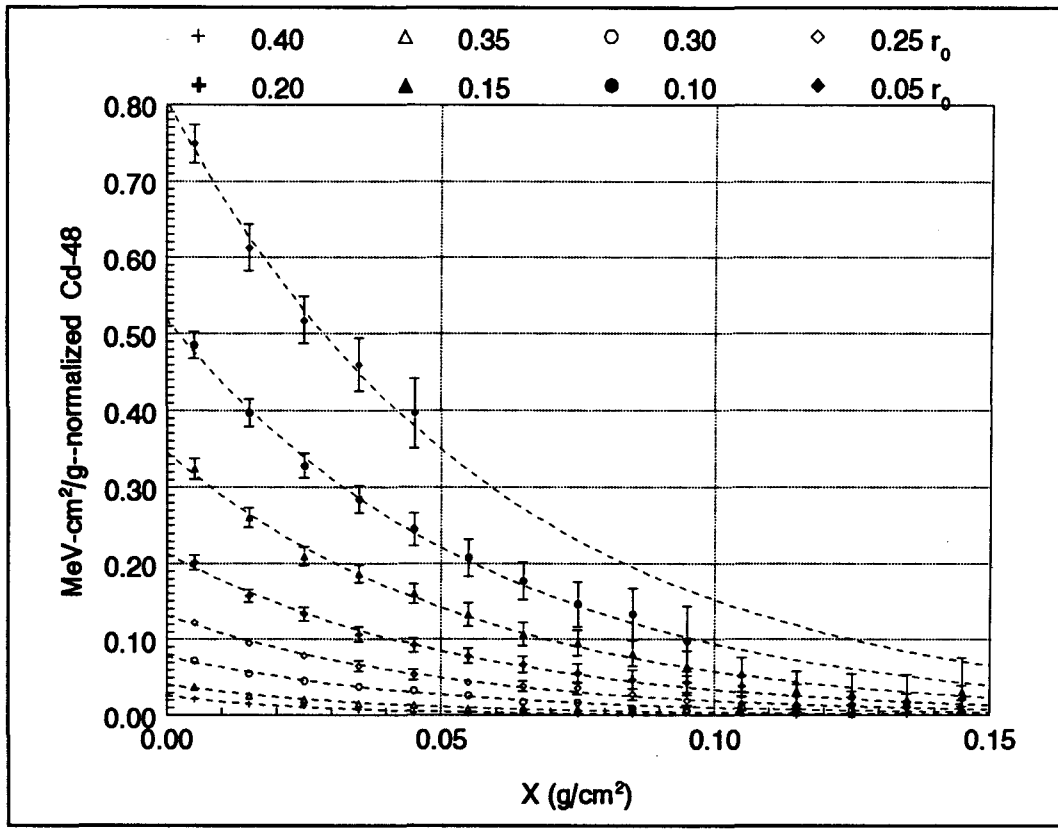

Fig.4.5. Dose backscattered relative to a water -$_{48}$Cd planar interface different source to interface distances r_0.

Table 4.3 Satturation backscatter factors.

Backscatterer	Bone	$_{13}$Al	$_{20}$Ca	$_{29}$Cu	$_{48}$Cd
Saturation Backscatter Coeff. a_0/D_h	0.0544 ± 0.0016	0.1459 ± 0.0028	0.2462 ± 0.0041	0.3380 ± 0.0034	0.4696 ± 0.0039

Appendix 4.2 presents individual graphs of backscatter factors for each type of interface and electron cutoff energy investigated. Fig. 4.6 shows the normalized dose backscatter factors versus source to interface distance r_0 for all backscatterers tested for 1keV cutoff energy runs. The saturation backscatter values used for normalization are given in Table 4.3.

The general trend observed for the backscatter coefficients consists of an exponential increase close to the source followed by a fairly constant saturation value for source to interface distances r_0 greater than 100mg/cm^2 (Fig. 4.6). For the low Z materials (Bone and Aluminum) a fall-off in backscatter coefficient was noticed at high r_0 for data resulting from runs with a 9keV electron energy cutoff. This trend proved to be only an artifact because it disappeared in the runs with a 1 keV electron energy cutoff (Appendix 4.2). The explanation for this effect is that low Z elements are weaker reflectors and the energy of the reflected spectrum is also lower for low Z elements (Snyman 1963). Consequently, the 9keV energy cutoff is significant compared to the backscattered energy and modifies the backscatter dose deposition. Only the results from the 1 keV cutoff runs have been considered for the final characterization of the backscatter factor.

A constant lower value was observed for the backscatter factor at r_0=50mg/cm^2 for each backscatterer tested compared to the rest of the r_0 values. In order to investigate the behavior of the backscatter factor at lower source to interface distances a set of two single scoring zone determinations were made for r_0 equal to 5 and 25mg/cm^2. All numerical data concerning these individual backscatter factor determinations are presented in Appendix

4.3. The backscatter factor values obtained confirmed the already noticed fall off trend for r_0 lower than 50mg/cm^2. For all tested materials the backscatter factors decrease exponentially to approximately forty percent of the saturation values for r_0=0mg/cm^2. The fall off starts at distances r_0 of about 70-80mg/cm^2. An exponential function was used to fit the variation of the normalized dose backscatter factors:

$$a_0/a_{0sat}=1+b\cdot\exp(-r_0/c) \qquad (4.9)$$

where r_0 is the source to interface distance in g/cm^2. Table 4.4 summarizes the fitting parameters and the fit statistics. Relationship 4.9 allows the calculation of backscatter factors close to the source when the saturation values are known.

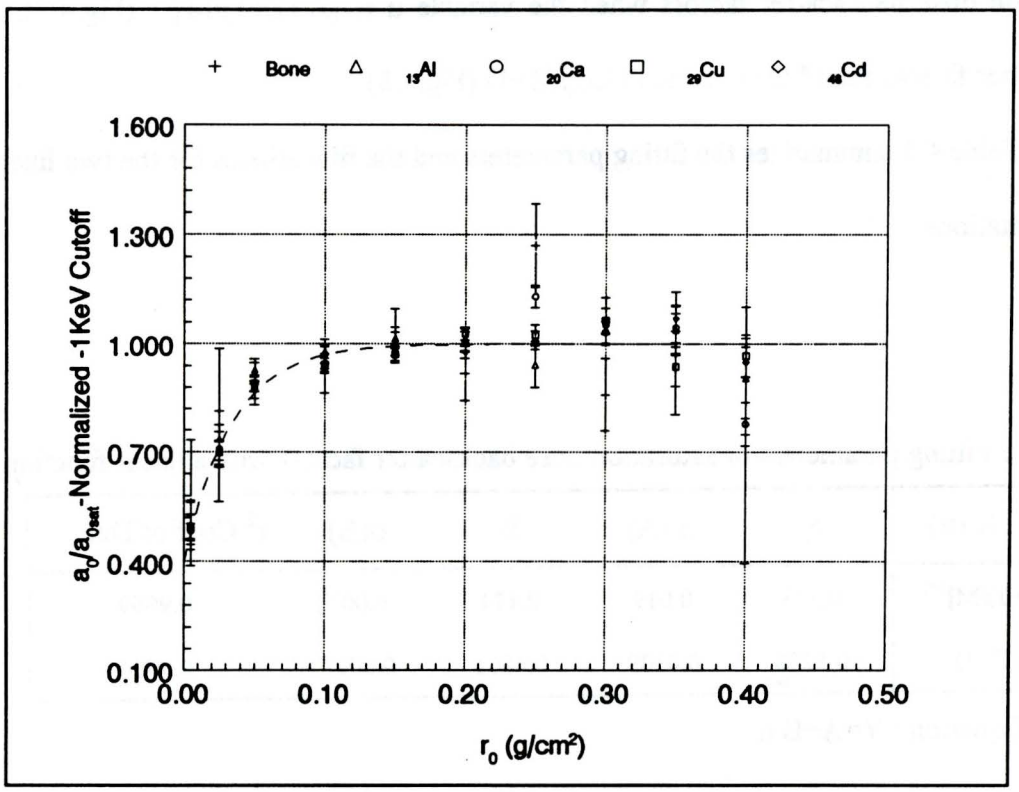

Fig. 4.6. The normalized dose backscatter factor versus source to interface distance r_0 for different interface compositions.

Table 4.4 Fitting parameters of the normalized backscater factors.

b	σ(b)	c	σ(c)	r^2 Coef.of Det.
-0.605	0.028	0.033	0.003	0.930

The backscatter factors defined in terms of electron number reflected were empirically fitted with a straight line by taking the quantities $[Z\ (Z+1)/M]^{1/2}$ (Mladjenovic M, 1973) or Log(Z+1) (Baily N, 1980) as the x-axis variable. Assuming a constant average stopping power for the backscattered spectrum the linearity should hold for dose backscatter coefficients. Indeed, a linear variation (A+B·u) was found by plotting the saturation dose backscatter factors when the variable u is $[Z\ (Z+1)/M]^{1/2}$ (Fig.4.7). An even better fit was found for u equal to Log(Z+1) (Fig.4.8)

Table 4.5 summarizes the fitting parameters and the fit statistics for the two linear representations.

Table 4.5 Fitting parameters of saturation dose backscatter factors with a linear function

Variable (u)	A	σ (A)	B	σ(B)	r^2 Coef.of Det.
$[Z*(Z+1)/M]^{1/2}$	-0.313	0.019	0.174	0.007	0.9969
Log(Z+1)	-0.5238	0.0109	0.5861	0.0091	0.9994

Equation : Y=A+B u

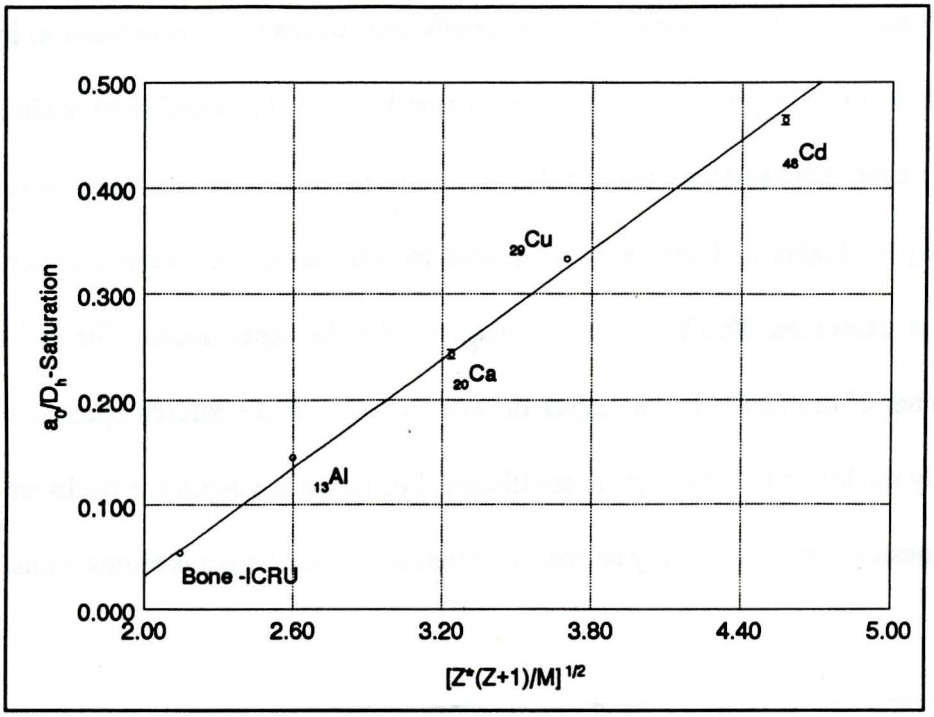

Fig.4.7 Saturation backscatter values a_0/D_h versus $[Z^*(Z+1)/M]^{1/2}$

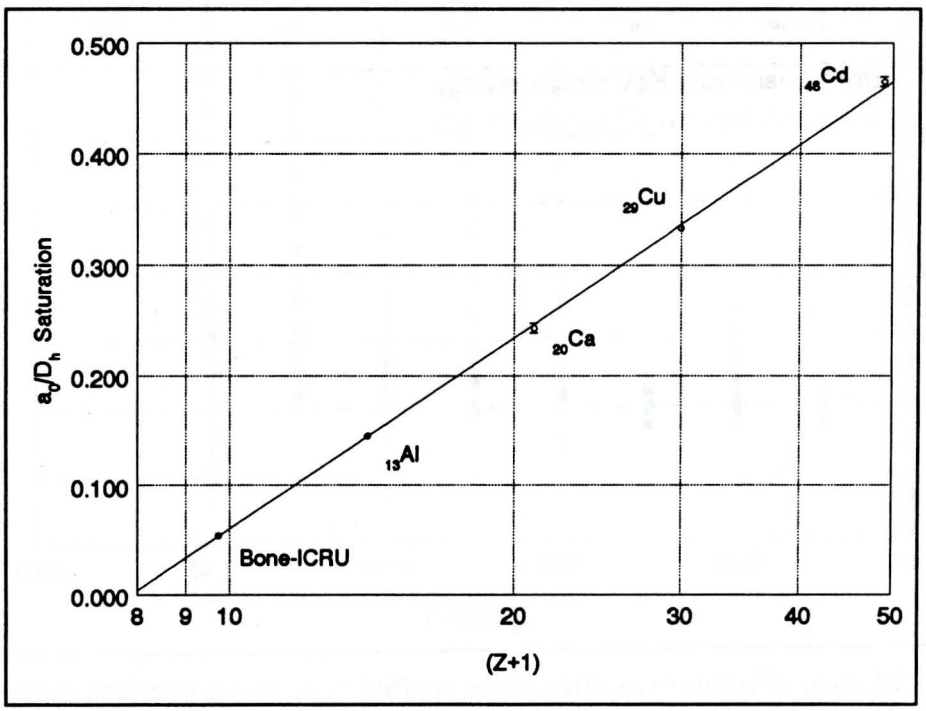

Fig.4.8 Saturation backscatter values a_0/D_h versus Log(Z+1)

The linear effective mass attenuation coefficient, which is the parameter a_1 in the fitting equation (4.7), is plotted as a function of r_0 in Fig. 4.9. The coefficient is almost a constant for every backscatterer up to a depth r_0 equal to 300mg/cm^2 and then increases exponentially for higher r_0. It also exhibits a small increase when the atomic number of the backscatterer decreases. This behavior is consistent with the expectations. The higher the atomic number of the scatterer, the higher the energy of the backscattered spectrum and subsequently the lower the attenuation coefficient. For moderate depth the backscattered spectrum doesn't vary significantly so that the attenuation coefficient is almost constant.

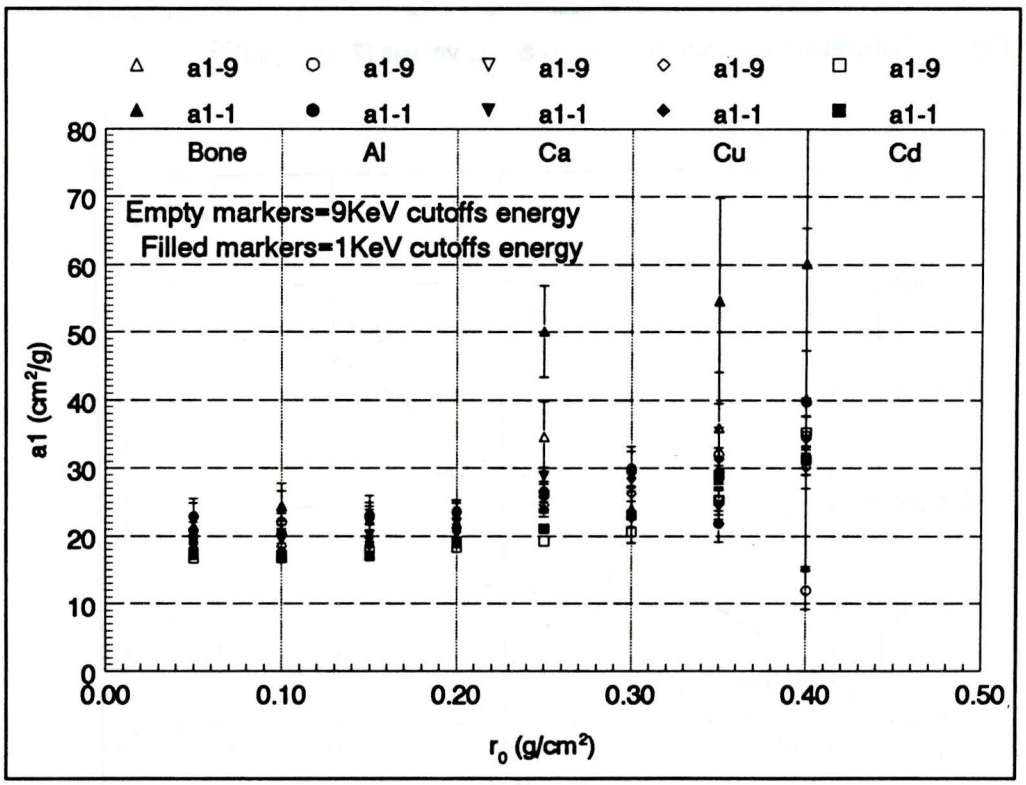

Fig. 4.9.Linear effective mass attenuation coefficient a_1 versus interface depth r_0, for 1keV and 9keV electron energies cutoff.

For high depth the energy of the electrons contributing to the backscattering is low, so that the backscattered spectrum energy is low, leading to an increased attenuation coefficient. An empirical fitting curve (4.8) was derived based on the data from 1keV electron energy cutoff runs that describes the variation with the interface depth r_0 (g/cm^2) and the scatterer atomic number Z.

$$a_1\left(cm^2/g\right)=\left[1.714-0.425\cdot\log(Z+1)\right]\cdot\left[15.504+0.724\cdot e^{\frac{r_0}{0.1258}}\right] \qquad (4.10)$$

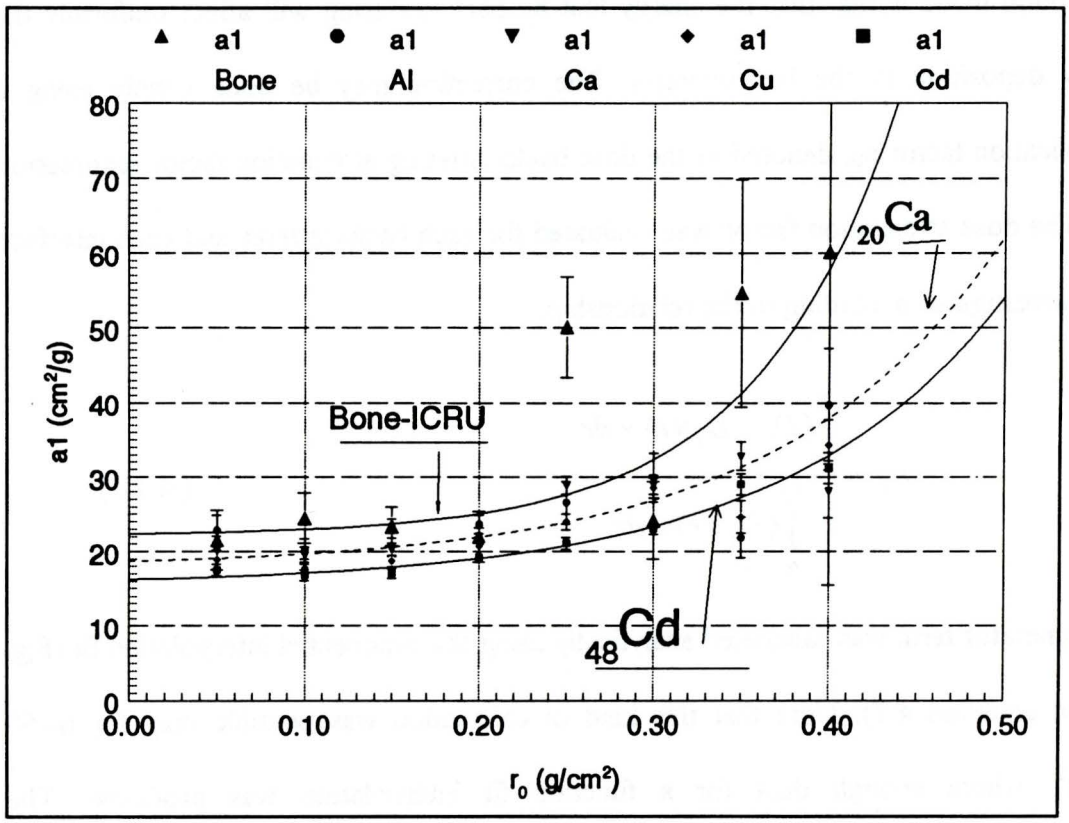

Fig.4.10. Curve fitting for the linear effective mass attenuation coefficient a_1 for data with 1keV cutoff runs.

Fig. 4.10 graphically compares the empirical curve calculated with the equation (4.10) for Ca (the dashed curve) to the curves resulting from data fit for the lowest and highest Z-media investigated, bone-ICRU and cadmium, respectively.

4.3.2 Depth Dose Deposition in Backscatterer

Along with the scaling a correction for the backscattered energy is necessary. The assumption made is that that the energy lost by backscattering will affect uniformly the energy deposition in the backscatterer .The correction may be done simply using a multiplication factor n_B, denoted as the dose backscattering attenuation factor (expression 4.1). The dose attenuation factor was evaluated for each backscatterer and each interface depth investigated according to the relationship:

$$1-n_B=\frac{\int_0^{r_0}(D_i-D_h)(r)\times dr}{\int_{r_0}^{+\infty}(D_h)(r)\times dr} \qquad (4.11)$$

The numerator term was calculated analytically using the exponential interpolation fit (Fig. 4.5 and equation 4.7). Note that this kind of calculation was possible only for r_0>50 mg/cm^2, where enough data for a function fit interpolation was produced. The denominator was evaluated by using numerical integration of the depth dose distribution

spline interpolation in water. A five degree polynomial and zero smoothing factor were used for the spline. The calculated values were averaged for each backscatter and the standard deviation of the average was estimated. A comprehensive picture of the calculations is presented in the Appendix 4.4

As a result, it was found that the attenuation coefficient does not depend upon the source to interface distance. It is a constant depending only upon the two materials forming the interface. Because the dose attenuation factor is physically strongly related to the backscattering phenomenon, the same dependency on atomic number as exhibited by the backscatter factor is expected.

Fig.4.11 and Fig. 12 show the linear dependency of the dose attenuation factor on the functions of Z introduced above for the dose backscatter factor.(Fig.4.7and Fig.4.8). The fit parameters are displayed in Table 4.6

Table 4.6 Fitting parameters of dose attenuation factors with a linear function

Variable (u)	M	σ (M)	N	σ(N)	r^2 Coef.of Det.
$[Z*(Z+1)/M]^{1/2}$	1.1852	0.0079	-0.0961	0.0028	0.9983
Log(Z+1)	1.293	0.016	-0.316	0.014	0.9963

Equation: Y=M+N u

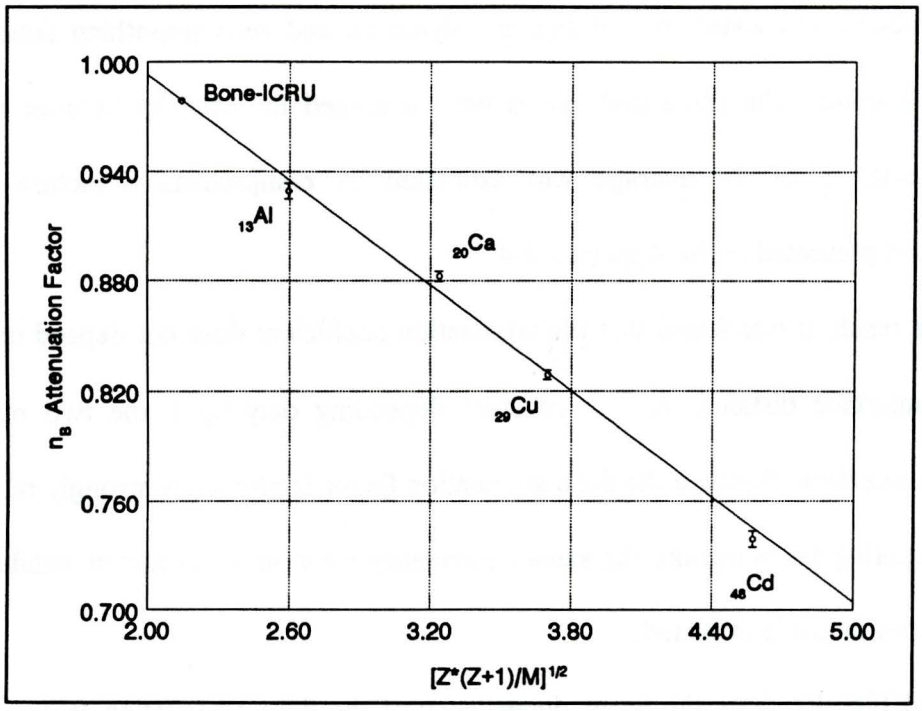

Fig. 4.11. Attenuation factor n_B versus atomic number and mass of the scatterers.

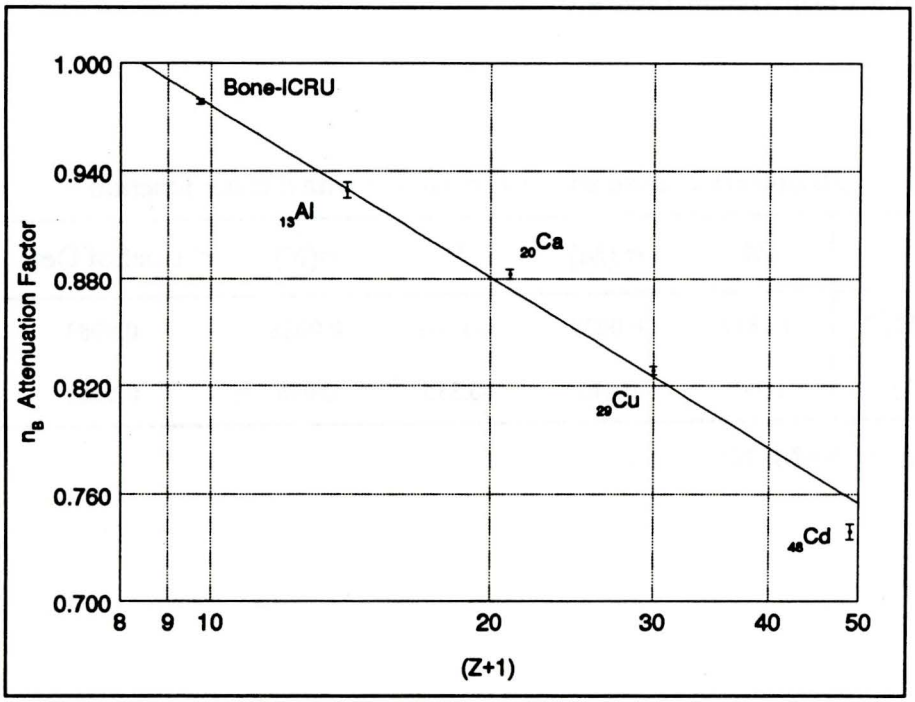

Fig. 4.12. Attenuation factor n_B versus log(Z+1) of the scatterers.

The fit of deriving the depth dose deposition for a water-cadmium interface from the dose in homogeneous water by scaling and correcting for the backscattering effect can be seen in Fig. 4.13.

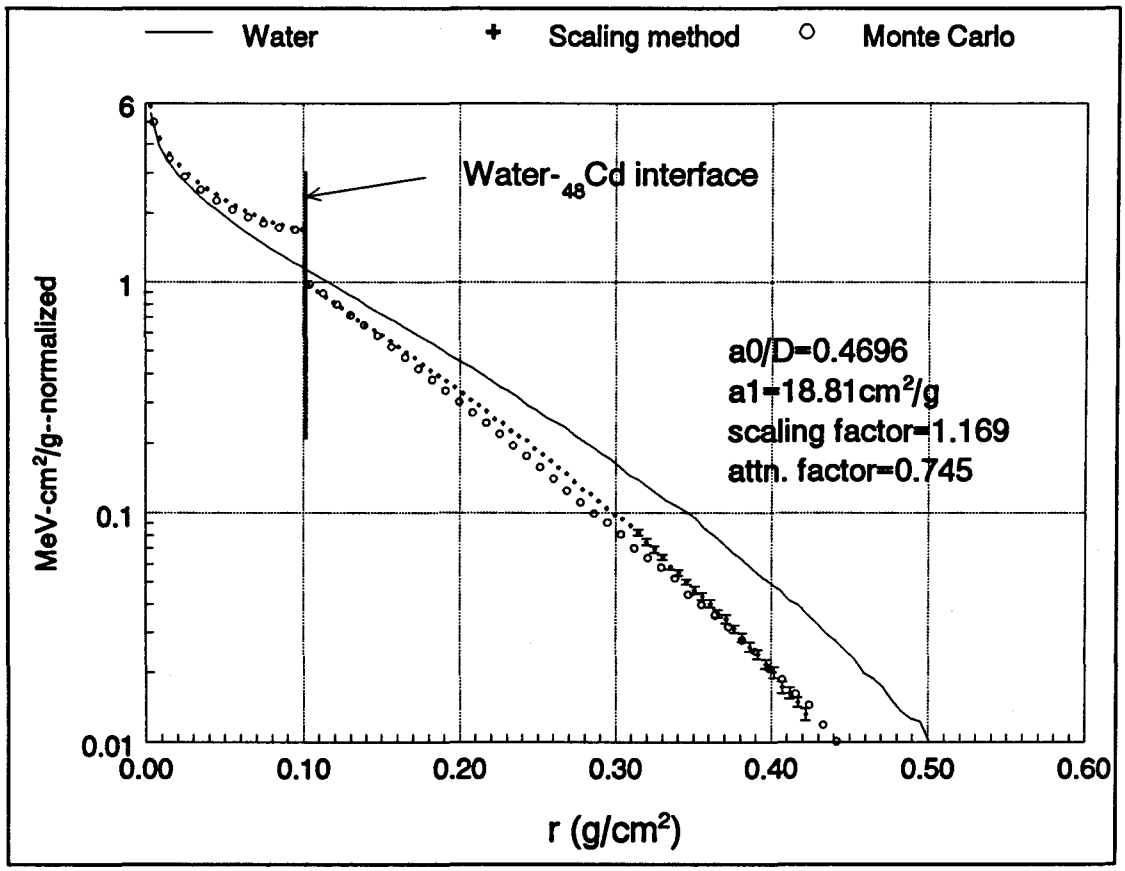

Fig.4.13 Dose depth deposition for a water-cadmium interface situated at a distance r_0=0.1g/cm^2 from the source.

4.4 Comments

This work offers a method of applying the scaling method for dose distribution derivations in dissimilar media with a planar interface from knowledge of the dose distribution in water. We are able to derive the depth dose distributions, in a plane geometry, for a P-32 radioisotopic source for a water-medium "i" interface. This is accomplished from the dose distribution in water by scaling and correcting for the dose backscattering, as described by the relationship (4.1). Medium "i" could be any element of known atomic number ($Z<50$), atomic mass and density. All the parameters necessary for the derivation can be determined by using coefficients resulting from the values given by Table 4.5 , Table 4.6 and equations 4.2 to 4.6 and 4.10. When the source-interface distance is lower than 100mg/cm^2 the dose backscattering factor a_0 and the attenuation factor n_B should be derived from the corresponding saturation values by using the supplementary correction given by the relationship 4.9.

To check the results the scaling method, as given by 4.1, was applied to three randomly chosen elements $_{40}$Zr, $_{32}$Ge, and $_{26}$Fe forming a planar interface with water. These media are different for the ones used for the determination of the method empirical coefficients. The depth dose depositions were derived based on the scaling method for interfaces situated at 100 and 350mg/cm^2. Fig. 4.14 to Fig 4.19 graphically compares the results of these derivations with Monte Carlo runs.

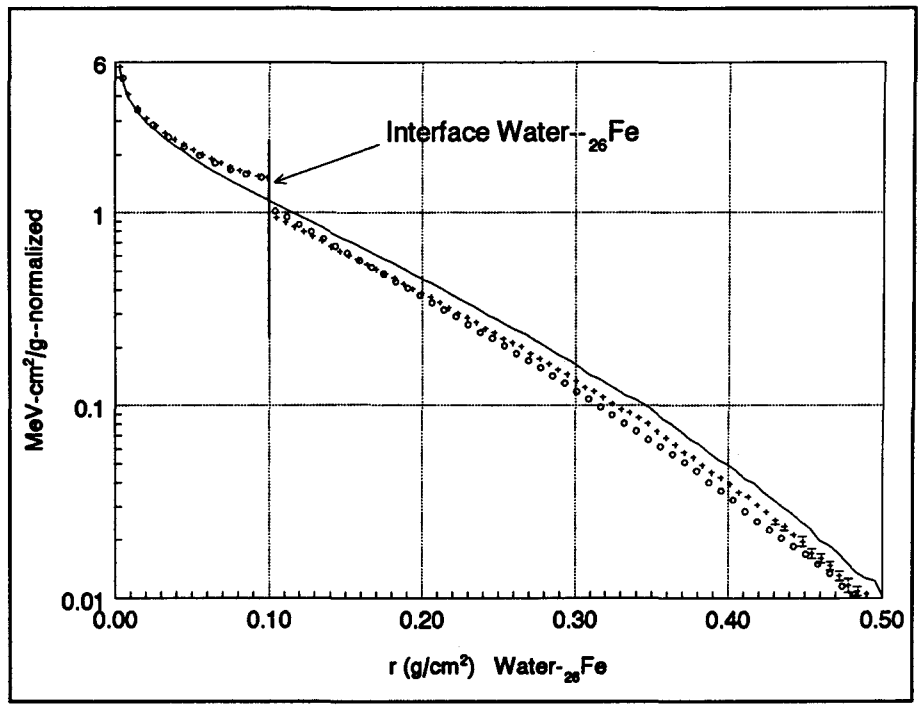

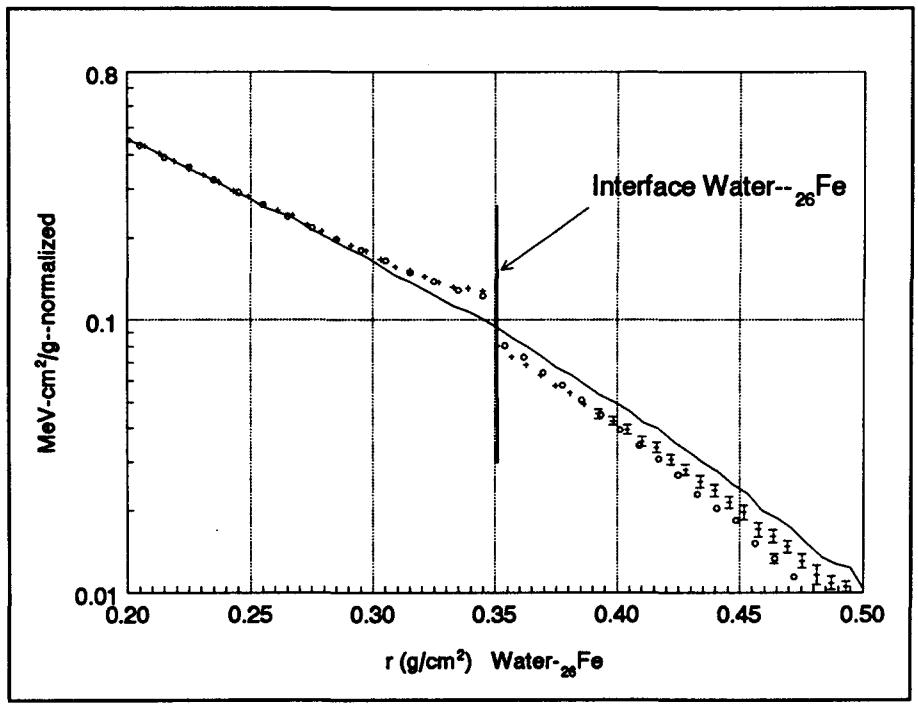

Fig. 4.14, Fig.4.15 Depth dose deposition for $_{26}$Fe calculated by scaling and backscatter correction (+) compared to exact Monte-Carlo calculations (o) and the homogeneous case of water (—).

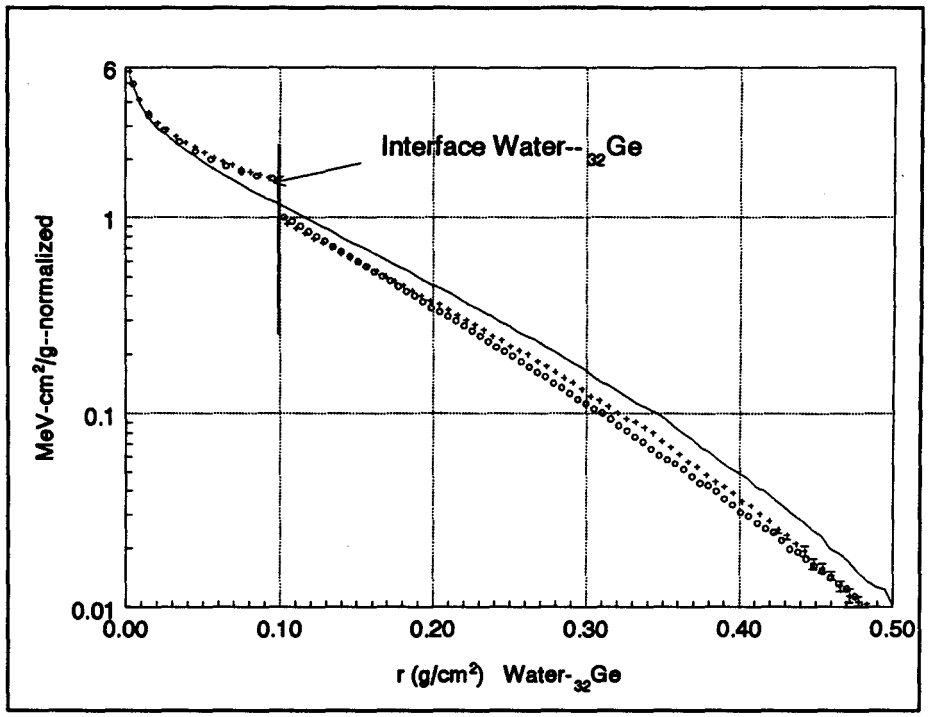

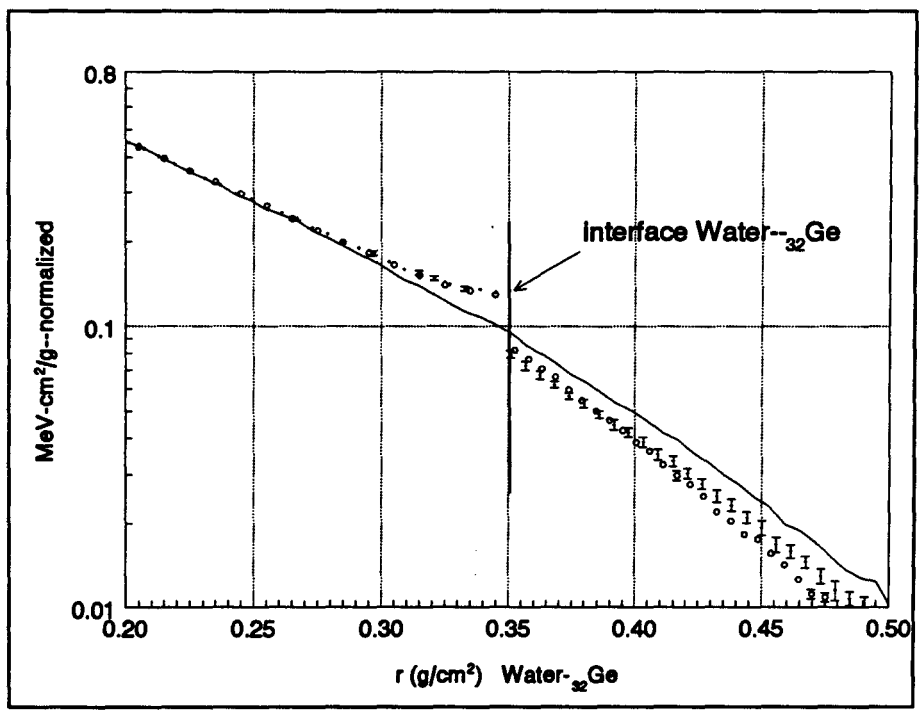

Fig. 4.16, Fig.4.17 .Depth dose deposition for $_{32}$Ge calculated by scaling and backscatter correction (+) compared to exact Monte-Carlo calculations (o) and the homogeneous case of water (—).

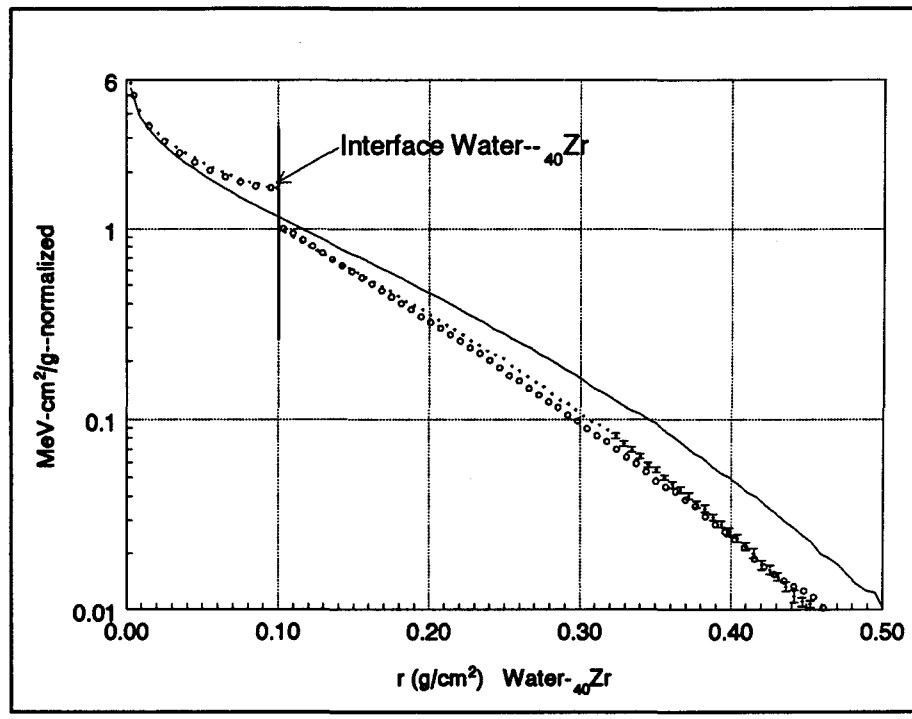

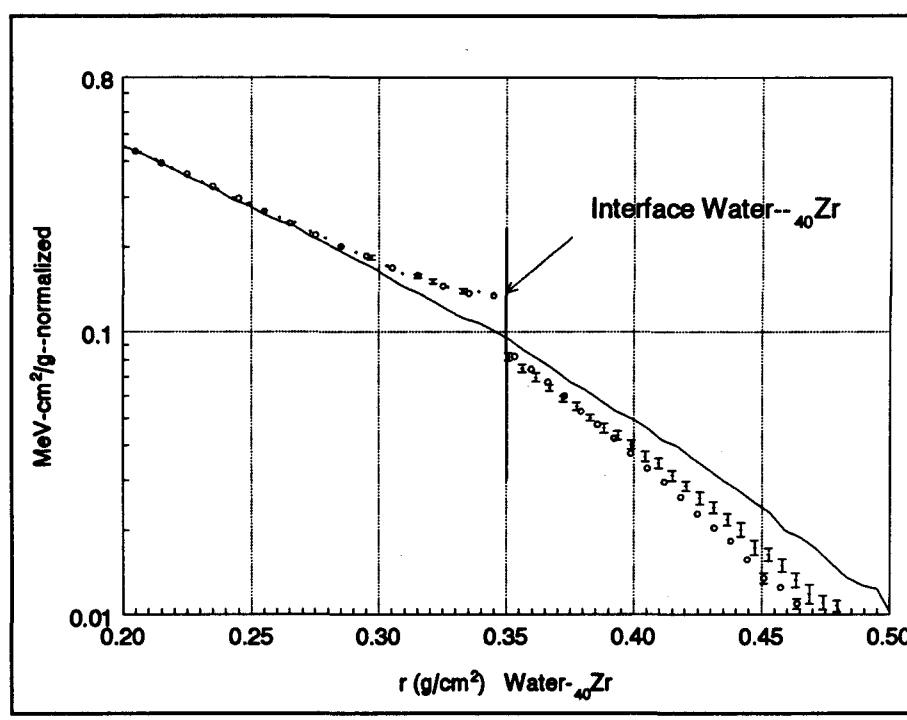

Fig. 4.18, Fig.4.19 .Depth dose deposition for $_{40}$Zr calculated by scaling and backscatter correction (+) compared to exact Monte-Carlo calculations (o) and the homogeneous case of water (—).

The differences are less than 3-4% (up to 5% is acceptable for practical radiotherapy) for a depth within which the dose deposited decreased by a factor of 100 from the initial value. The highest discrepancy reaches 10-15% at approximately 300mg/cm^2 depth, but at this point already 96% of the initial energy is deposited.

The fit of the backscattered dose D_d (x) (eq. 4.7) with an exponential function is consistent with the experimental observation that transmission of beta particles is approximately an exponential (Knoll 1992). Assuming a constant average stopping power for the backscattered spectrum, the same approximate exponential behavior should be observed for the dose backscattered.

An exponential variation for any partial spectrum is also predicted in the "Two Group" method , discussed in the section 2.7, equation 2.29.

The behavior found in our Monte Carlo investigations for the backscatter factor a_0 is consistent with the results of the "Two Group" method, equations 2.30 and 2.31. This factor reaches a constant saturation value but exhibits a fall off for very small source-interface distances due to a very small diffusion component of the flux. We were able to compare the saturation backscatter factors given by the "Two Group" method with the results of the Monte Carlo calculations and the results from the empirical linear relationship found in this work (coefficients given into Table 4.5)

Table 4.7 compares the saturation backscatter factor calculated based on the two group method data (equation 2.31), Monte Carlo results (Appendix 4.2) , and the linear

Table 4.7 Saturation backscatter factors calculated whith three different methods.

	"Two Group"	Monte Carlo	a0+a1*log(Z+1)
Cd (Z=48)	0.47	0.465±0.004	0.460
Cu (Z=29)	0.33	0.333±0.003	0.336
Al (Z=13)	0.14	0.145±0.003	0.145

relationship with the coefficients from Table 4.5. It should be mentioned that the "Two Group" method uses experimental data for the determination of the empirical fitting coefficients. A very good agreement was found among the three sets of data.

CHAPTER 5.

5. Conclusions

The accuracy of the scaling factor method was investigated in planar geometry using a generalized chi-squared test for two similar atomic number media, water and bone-ICRU, for electron energies ranging from 0.1 to 2 MeV. The discrepancies detected are less than 5% up to at least 60% of the range in bone, a depth within which 95% of the initial energy is deposited. A scaling factor of water to bone, η_w=(972.0±1.2) 10^{-3}, was determined. This new value is consistent with the one cited in literature but the accuracy of the determination proved to be almost an order of magnitude higher.

For the point geometry the accuracy of the scaling method is within 5% up to 60% of the range in bone, less than to 8% up to a depth of 85% of the range in bone and higher for the rest.

A universal modulation function was defined, which can improve the method of scaling for deriving the monoenergetic dose kernels in bone from those in water. The modulation functions were determined in a six degree polynomial representations for both geometries, plane F(x) and point M(x), for a dimensionless depth relative to the range in bone.

This work offers a method of applying the scaling method together with a correction for backscattering effect for dose distribution derivations in dissimilar media, a planar interface, from knowledge of the dose distribution in water. All the necessary parameters were determined so that one can predict the depth dose distributions in a plane geometry for a P-32 radioisotopic source for a water-medium "i" interface. Medium "i" could be any element of known atomic number ($Z<50$), atomic mass and density. The method was checked on three randomly chosen elements $_{40}Zr$, $_{32}Ge$, and $_{26}Fe$ forming planar interfaces with water at 100 and 350mg/cm^2. Discrepancies less than 5% were detected (acceptable for practical radiotherapy) for depth within which more than 95% of the initial energy is deposited. We assume that similar calculations could be done for any beta radioisotope of clinical interest.

The accuracy determined recommends the scaling factor method as a possible instrument for fast estimates in solving problems of routine dosimetry with planar geometry. Future work should be done to develop procedures to apply the scaling factor method to non-planar geometries and to more than one closely spaced boundary.

APPENDIX 4.1

The quantification of the P-32 beta spectrum.

Maximum energy: $E_{max.}$=1.708 MeV

Average energy: $E_{ave.}$=0.694 MeV

(Lederer 1978)

Energy (MeV)	Percentage /100	Cumulative Pecentage /100
0.009	0.000000	0.0000
0.100	0.037302	0.0373
0.200	0.055042	0.0923
0.300	0.069419	0.1617
0.400	0.080780	0.2425
0.500	0.088942	0.3314
0.600	0.093710	0.4251
0.700	0.094991	0.5201
0.800	0.092829	0.6129
0.900	0.087413	0.7003
1.000	0.079088	0.7794
1.100	0.068351	0.8478
1.200	0.055858	0.9037
1.300	0.042423	0.9461
1.400	0.029016	0.9751
1.500	0.016765	0.9919
1.600	0.006956	0.9989
1.708	0.001114	1.0000

Average beta energy calculated with the continuous spectrum (Fig. 4.2):

$E_{ave.\ cont.}$=0.6933 MeV

Average beta energy calculated after quantification (Table above):

$E_{ave.q.}$ = 0.6934 MeV

APPENDIX 4.2

The backscatter factors versus the source to interface distance r_0.

The determination was done by a weighted fit of the twenty data (for 9 and 1 keV cutoffs energy runs) with a function of the type: $y=c_0+c_1 \exp(-x/c_2)$. The function is represented by a continuous line in the graphs. The dotted line represents the saturation backscatter values, which are the c_0 coefficients in the fitting equation.

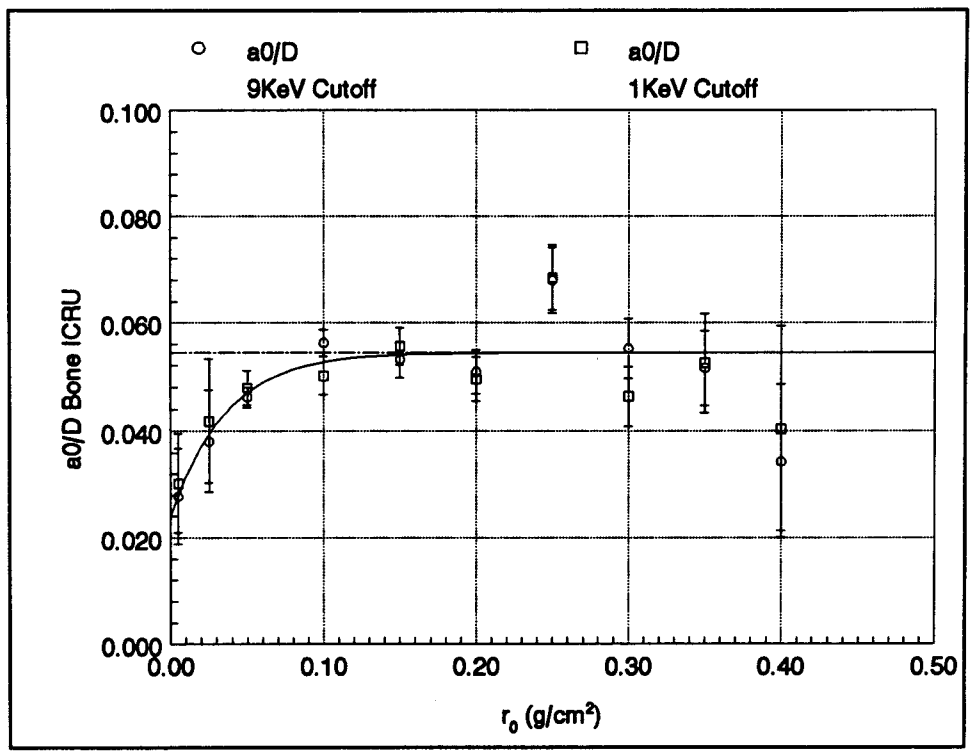

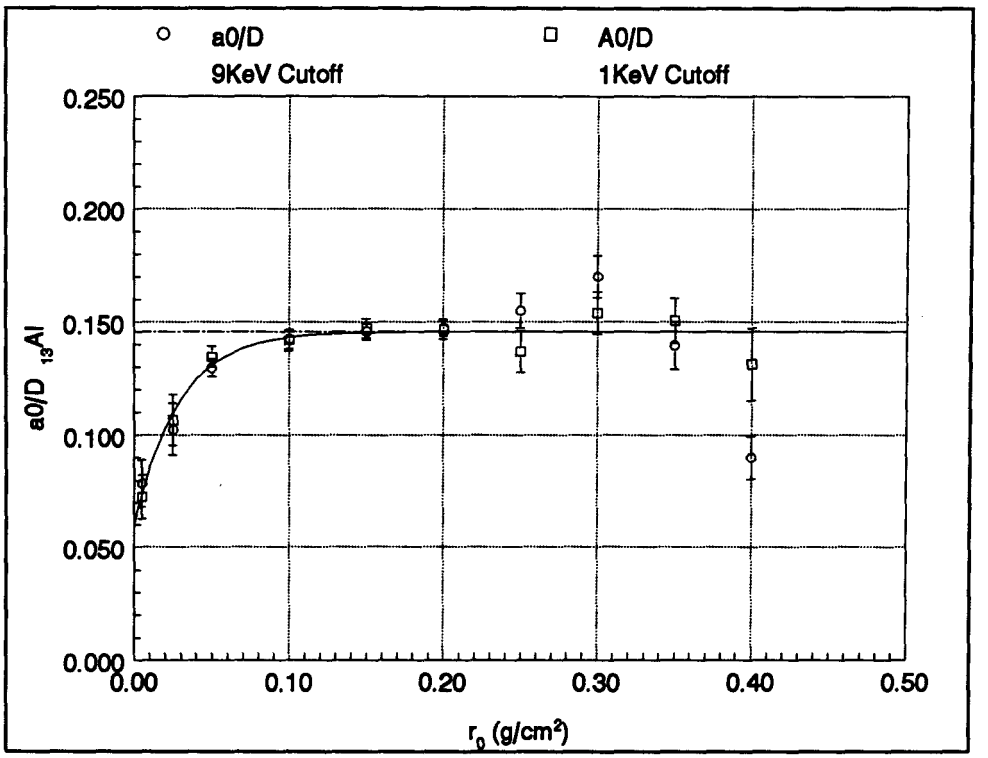
a0/D
9KeV Cutoff
A0/D
1KeV Cutoff
0.250
0.200
0.150
0.100
0.050
0.000
a0/D 13Al
0.00
0.10
0.20
0.30
0.40
0.50
r0 (g/cm2)

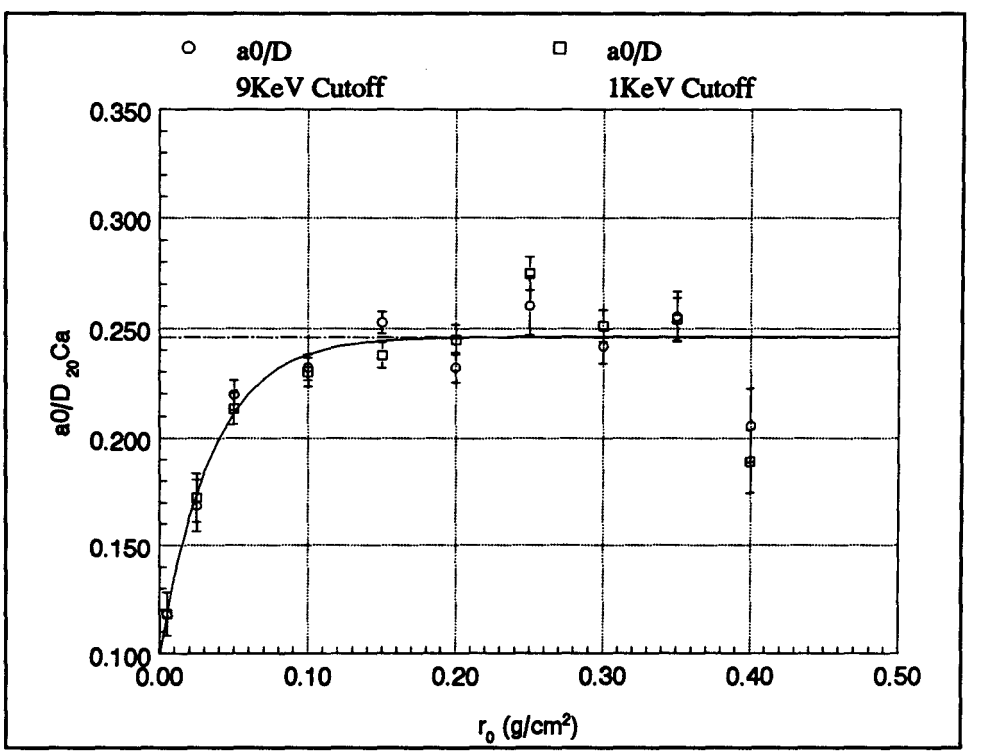
a0/D
9KeV Cutoff
a0/D
1KeV Cutoff
0.350
0.300
0.250
0.200
0.150
0.100
a0/D 20Ca
0.00
0.10
0.20
0.30
0.40
0.50
r0 (g/cm2)

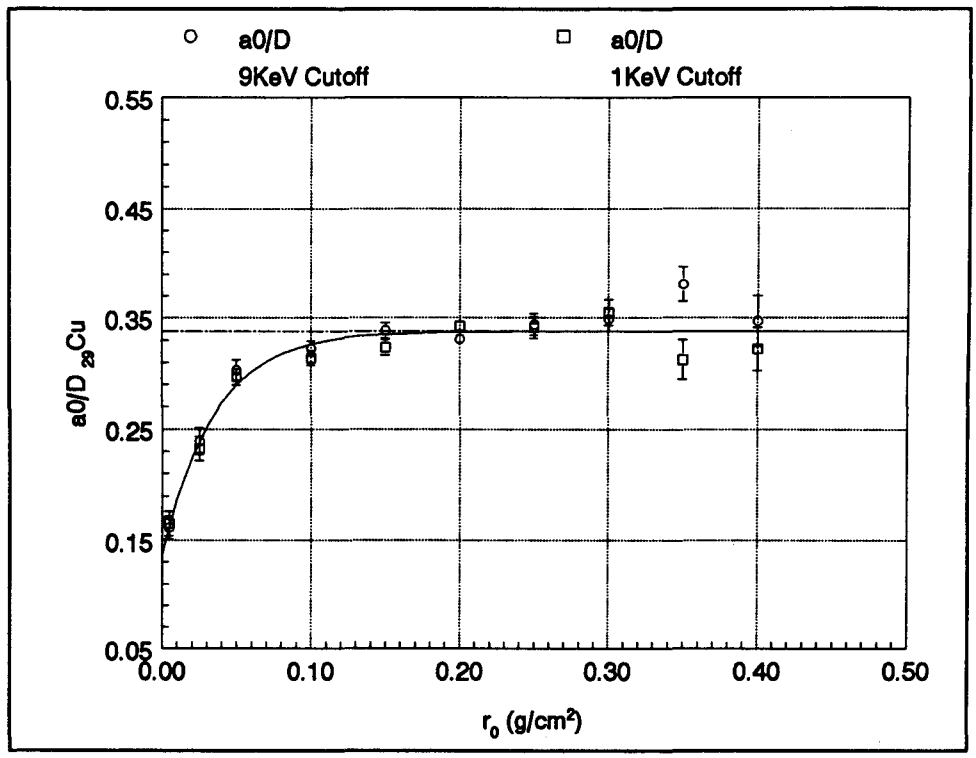
a0/D
9KeV Cutoff
a0/D
1KeV Cutoff
0.55
0.45
0.35
0.25
0.15
0.05
a0/D 29Cu
0.00
0.10
0.20
0.30
0.40
0.50
r0 (g/cm2)

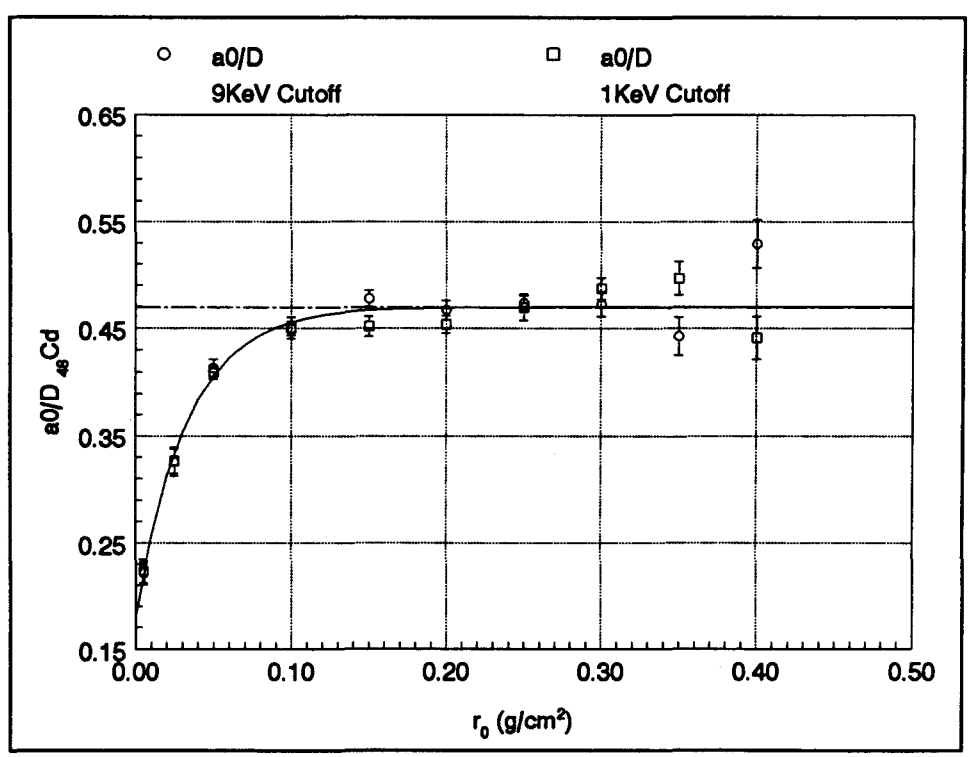
a0/D
9KeV Cutoff
a0/D
1KeV Cutoff
0.65
0.55
0.45
0.35
0.25
0.15
a0/D 48Cd
0.00
0.10
0.20
0.30
0.40
0.50
r0 (g/cm2)

The fitting according to the equation 4.7 of the dose difference $D_d(x)$ for different source to interface distances r_0 for Bone, Al, Ca, and Cu as backscatterer.

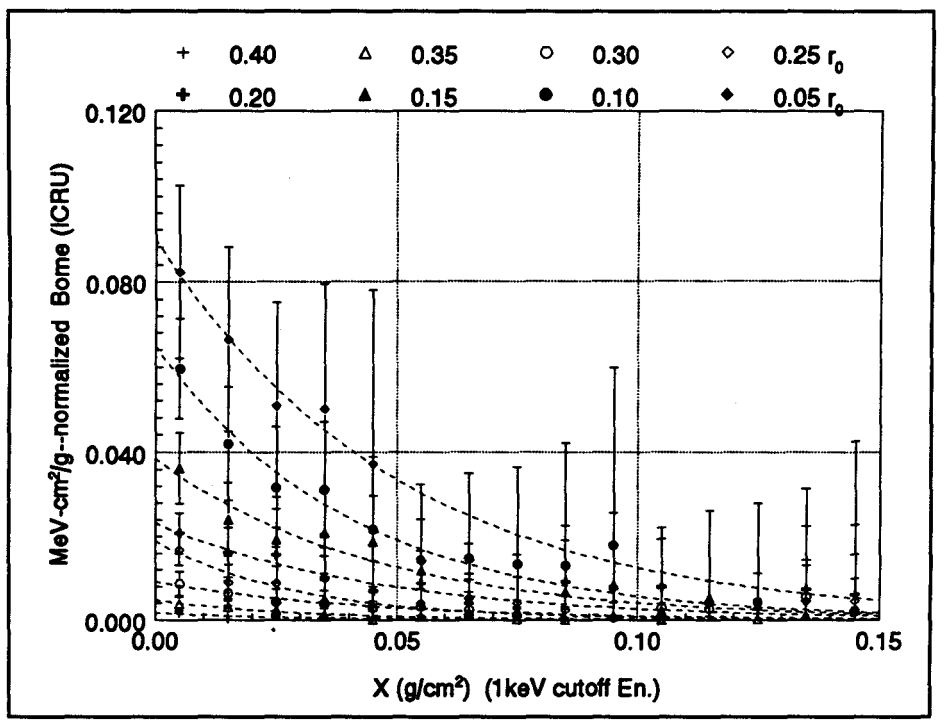

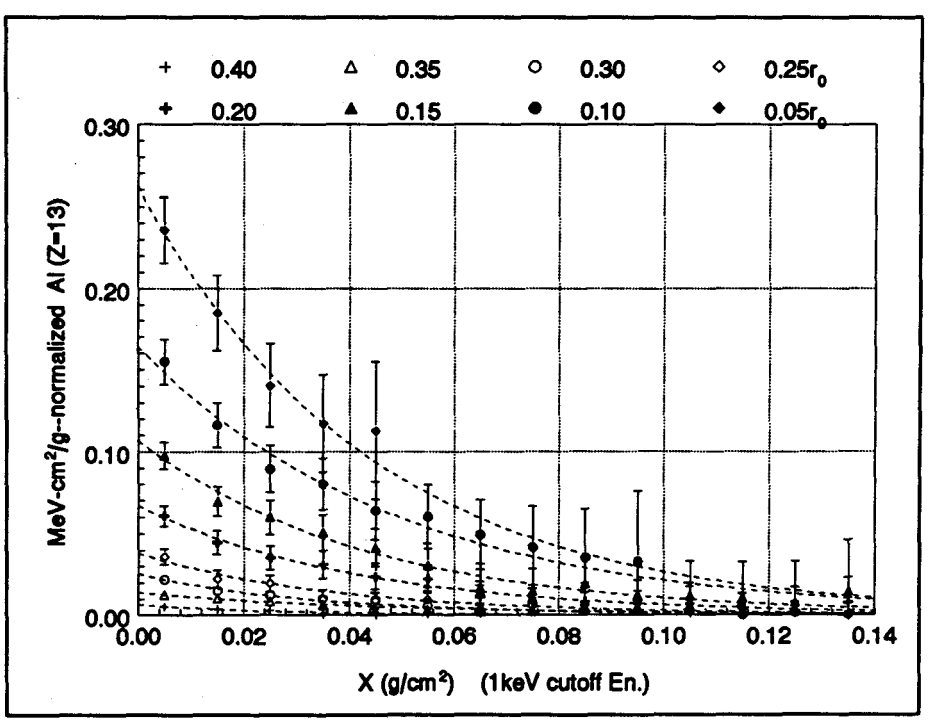

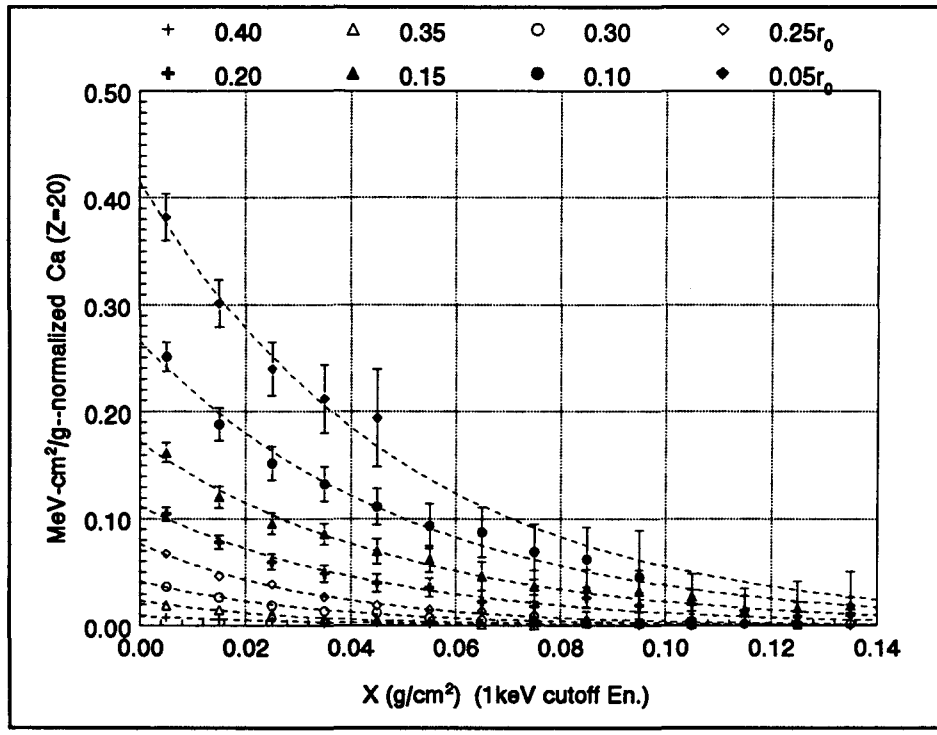
+ 0.40
△ 0.35
○ 0.30
◇ 0.25r0
+ 0.20
▲ 0.15
● 0.10
◆ 0.05r0
MeV-cm²/g--normalized Ca (Z=20)
0.00
0.10
0.20
0.30
0.40
0.50
0.00
0.02
0.04
0.06
0.08
0.10
0.12
0.14
X (g/cm²) (1keV cutoff En.)

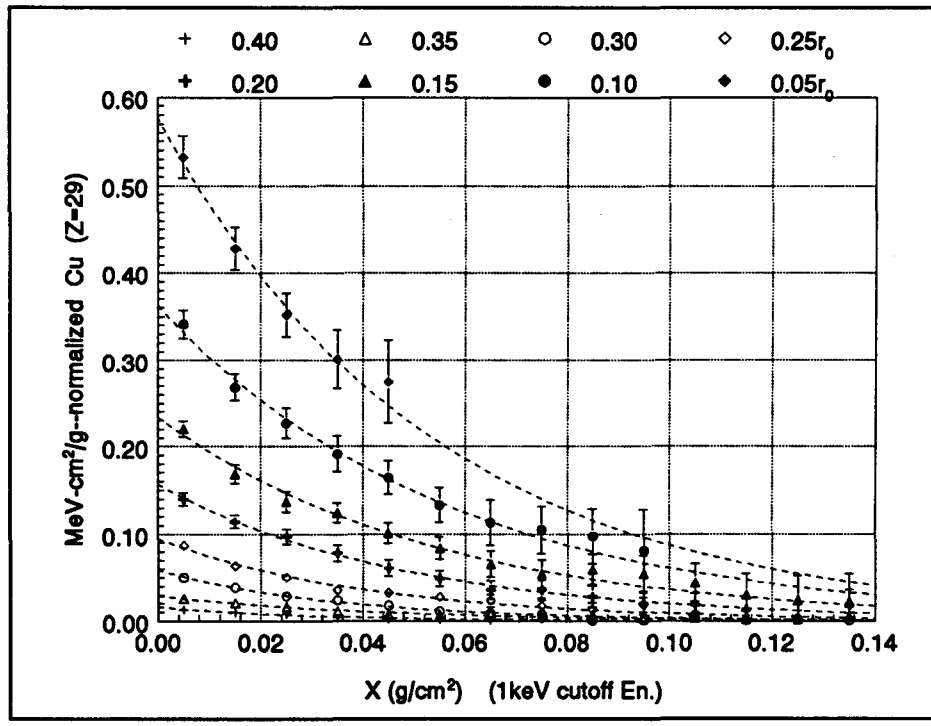
+ 0.40
△ 0.35
○ 0.30
◇ 0.25r0
+ 0.20
▲ 0.15
● 0.10
◆ 0.05r0
MeV-cm²/g--normalized Cu (Z=29)
0.00
0.10
0.20
0.30
0.40
0.50
0.60
0.00
0.02
0.04
0.06
0.08
0.10
0.12
0.14
X (g/cm²) (1keV cutoff En.)

APPENDIX 4.3

Individual zone backscattering factor determination for source to interface distances r_0=5mg/cm^2 (Zone1) and, r_0=25mg/cm^2 (Zone3).

Backscatering coefficients for the scoring zones 1 and 3

ZONE 1 5mg/cm^2

Dose in water =4.8776 +/- 0.6% Mev-cm^2/g-source particle

CUTOFFS En. =0.009 MeV

Element / Z	Dose *	Error(%)	Backscatt.	Error
Cd / 48	5.9583418	0.66	0.222	0.011
Cu / 29	5.6648574	0.65	0.161	0.010
Ca / 20	5.4545425	0.65	0.118	0.010
Al / 13	5.2610731	0.75	0.079	0.010
Bone / 8.74	5.0133664	0.65	0.028	0.009

CUTOFFS En.= 0.001 MeV

Element / Z	Dose *	Error(%)	Backscatt.	Error
Cd / 48	5.9670043	0.67	0.223	0.011
Cu / 29	5.6834611	0.72	0.165	0.011
Ca / 20	5.4546771	0.66	0.118	0.010
Al / 13	5.2311069	0.69	0.072	0.010
Bone / 8.74	5.0252528	0.67	0.030	0.009

ZONE 3 25mg/cm^2

Dose in water =2.7456 +/- 0.6% Mev-cm^2/g-source particle

CUTOFFS En.=0.009 MeV

Element / Z	Dose *	Error(%)	Backscatt.	Error
Cd / 48	3.6402661	0.81	0.326	0.013
Cu / 29	3.4020658	0.74	0.239	0.012
Ca / 20	3.2080160	0.84	0.168	0.012
Al / 13	3.0271293	0.83	0.103	0.011
Bone / 8.74	2.8501691	0.67	0.038	0.009

CUTOFFS En.= 0.001 MeV

Element / Z	Dose *	Error(%)	Backscatt.	Error
Cd / 48	3.6418405	0.61	0.326	0.011
Cu / 29	3.3837801	0.65	0.232	0.011
Ca / 20	3.2181292	0.77	0.172	0.011
Al / 13	3.0385284	0.81	0.107	0.011
Bone / 8.74	2.8602876	0.69	0.042	0.010

* Dose in Mev-cm^2/g-source particle

APPENDIX 4.4

Attenuation factor determination was done according to the equation (4.11). The integral of the dose depth deposition in water was performed by numerical integration of the spline interpolation of data from a $2*10^6$ histories Monte Carlo run.

The coefficients a0 and a1, defined by the expression (4.6) and used for the attenuation factor determinations, are in units of:

[a0] = MeV-cm^2/g- normalized per beta decay

[a1] = cm^2/g

Depth (mg/cm^2)	Dose integral in water (MeV-cm^2/g)
50	0.19164601
100	0.11661770
150	0.07060607
200	0.04165699
250	0.02363021
300	0.01280001
350	0.00651321
400	0.00306488

Attenuation factor n_B determination

Cd Z=48

----------A.-Cutoff Energy =1keV---------- Attn. A.

Zone (mg/cm^2)	r2Coef of Det.	a0	sigma a0	a1	sigma a1	
50	0.9956	0.797485	0.011347	17.488930	0.775007	0.7620644
100	0.9903	0.519649	0.010828	16.798093	0.742986	0.7347315
150	0.9914	0.321718	0.006436	17.074623	0.652526	0.7331408
200	0.9945	0.207129	0.003266	19.210409	0.529476	0.7411689
250	0.9891	0.129995	0.002977	21.099407	0.799522	0.7392713
300	0.9933	0.080533	0.001400	23.060418	0.724300	0.7271673
350	0.9824	0.046174	0.001335	29.023088	1.396805	0.7557362
400	0.9525	0.021915	0.000930	31.216670	2.092651	0.7709442
					Average A	0.7455281
					STDS	0.0054917
					% STDS	0.74

----------B.-Cutoff Energy =9keV---------- Attn. B.

Zone (mg/cm^2)	r2Coef. of Det.	a0	sigma a0	a1	sigma a1	
50	0.9919	0.805278	0.014994	16.706354	0.989479	0.7484847
100	0.9968	0.519005	0.006288	17.08472	0.444870	0.7395051
150	0.9956	0.345752	0.005138	17.857065	0.467347	0.7257715
200	0.9945	0.213106	0.003561	18.365704	0.523364	0.7214519
250	0.9957	0.131346	0.001766	19.307928	0.461217	0.7121186
300	0.9887	0.078090	0.001681	20.642171	0.723447	0.7044508
350	0.9756	0.041170	0.001536	25.365427	1.573891	0.7508024
400	0.9583	0.026271	0.001070	35.220528	2.445399	0.7566299
					Average B	0.7324019
					STDS	0.0068023
					% STDS	0.93

Atten.-C (averaged A and B)

n =0.7390 ± 0.0044

Cu Z=29

----------A.-Cutoff Energy =1keV----------

Zone (mg/cm^2)	r2Coef of Det.	a0	sigma a0	a1	sigma a1	Attn. A.
50	0.9893	0.578115	0.013439	18.913335	1.289491	0.8405053
100	0.9928	0.362312	0.006666	17.815297	0.699772	0.8256086
150	0.9908	0.233986	0.004907	18.714109	0.782511	0.8229163
200	0.9954	0.156368	0.002430	20.694449	0.58976	0.8186130
250	0.9861	0.094556	0.002550	23.98440	1.044074	0.8331629
300	0.9792	0.058624	0.001787	28.51345	1.350783	0.8393742
350	0.9409	0.029038	0.001609	24.623597	2.156672	0.8189409
400	0.9289	0.015991	0.000926	34.314027	3.379564	0.8479486
					Average	0.8308837
					STDS	0.0038858
					% STDS	0.47

----------B.-Cutoff Energy =9keV----------

Zone (mg/cm^2)	r2Coef. of Det.	a0	sigma a0	a1	sigma a1	Attn. B.
50	0.9823	0.589664	0.017371	18.282035	1.635688	0.8317015
100	0.9921	0.372013	0.007302	18.591892	0.772851	0.8284187
150	0.9927	0.245203	0.004630	19.101634	0.690886	0.8181919
200	0.9952	0.150952	0.002434	21.013545	0.587708	0.8275546
250	0.9852	0.095375	0.002542	24.539401	1.105170	0.8355238
300	0.9856	0.057605	0.001559	26.291607	1.153387	0.8288280
350	0.9729	0.035344	0.001379	31.325023	1.757300	0.8267675
400	0.8964	0.017233	0.001100	30.120425	3.045465	0.8133250
					Average	0.8262889
					STDS	0.002539
					% STDS	0.31

Atten.-C (averaged A and B)

n =0.8286 ± 0.0023

Ca Z=20

----------A.-Cutoff Energy =1keV----------

Zone (mg/cm^2)	r2Coef of Det.	a0	sigma a0	a1	sigma a1	Attn. A.
50	0.9808	0.415744	0.013679	20.182870	1.899823	0.8925161
100	0.9848	0.265266	0.007490	19.480080	1.146030	0.8832313
150	0.9897	0.171982	0.004017	20.249153	0.90052	0.8797087
200	0.9865	0.111687	0.003023	22.076083	1.099452	0.8785514
250	0.9892	0.076192	0.001901	28.894492	1.208517	0.8884096
300	0.9852	0.041495	0.001099	28.919449	1.287180	0.8879026
350	0.9762	0.023617	0.000863	32.831386	1.929110	0.8895564
400	0.8859	0.009389	0.000713	28.134618	3.616160	0.8911158
					Average	0.8863740
					STDS	0.0018532
					% STDS	0.21

----------B.-Cutoff Energy =9keV----------

Zone (mg/cm^2)	r2Coef. of Det.	a0	sigma a0	a1	sigma a1	Attn. B.
50	0.9825	0.427929	0.013034	19.403618	1.722638	0.8849228
100	0.9895	0.267623	0.006371	19.495630	0.993869	0.8822877
150	0.9943	0.183211	0.003110	22.18322	0.724143	0.8830271
200	0.9842	0.105857	0.002992	20.743226	1.013880	0.8774946
250	0.9518	0.072132	0.003615	26.018809	2.086636	0.8826797
300	0.9771	0.039944	0.001236	22.599299	1.251525	0.8619151
350	0.9507	0.023726	0.001029	25.210944	1.993010	0.8555091
400	0.8583	0.010206	0.000823	34.674823	5.688357	0.9039654
					Average	0.8789752
					STDS	0.0052524
					% STDS	0.60

Atten.-C (averaged A and B)

n =0.8827 ± 0.0028

Al Z=13

----------A.-Cutoff Energy =1keV----------

Zone (mg/cm^2)	r2Coef of Det.	a0	sigma a0	a1	sigma a1	Attn. A.
50	0.9846	0.262113	0.008519	22.896976	1.981213	0.9402675
100	0.9802	0.163816	0.005440	20.321022	1.378837	0.9308732
150	0.9862	0.106634	0.003028	23.072426	1.287175	0.9345424
200	0.9842	0.066935	0.001920	23.623002	1.243747	0.9319810
250	0.9298	0.037904	0.002531	26.563120	2.861936	0.9396137
300	0.9349	0.025461	0.001535	29.938855	3.290410	0.9335599
350	0.9155	0.013997	0.000916	21.861422	2.703164	0.9016981
400	0.7121	0.006517	0.000792	39.731346	7.543046	0.9464819
					Average	0.9323772
					STDS	0.0047496
					% STDS	0.51

----------B.-Cutoff Energy =9keV----------

Zone (mg/cm^2)	r2Coef. of Det.	a0	sigma a0	a1	sigma a1	Attn. B.
50	0.9911	0.256137	0.007442	21.789923	1.197271	0.9386638
100	0.9867	0.164320	0.004739	22.117354	1.244749	0.9362922
150	0.9897	0.105551	0.002596	22.836623	1.094260	0.9345381
200	0.9912	0.067220	0.001550	23.575448	0.984955	0.9315536
250	0.9531	0.043025	0.002079	26.022267	2.027338	0.9300306
300	0.9465	0.028119	0.001485	29.554873	2.886138	0.9256706
350	0.9095	0.012996	0.000968	32.032969	3.979506	0.9377101
400	0.5507	0.004467	0.000471	11.980496	2.811418	0.8783457
					Average	0.9266006
					STDS	0.0070604
					% STDS	0.76

Atten. Al (A and B averaged)

n =0.9295 ± 0.0043

Bone -
ICRU

----------A.-Cutoff Energy =1keV---------- Attn. A.

Zone (mg/cm^2)	r2Coef of Det.	a0	sigma a0	a1	sigma a1	
50	0.9322	0.093291	0.006137	21.514730	3.985442	0.9773742
100	0.9337	0.057867	0.004046	24.455015	3.346566	0.9797092
150	0.9384	0.040259	0.002487	23.376340	2.594167	0.9756082
200	0.8536	0.022595	0.001839	21.935710	3.406606	0.9752729
250	0.8968	0.018989	0.001696	50.123028	6.738489	0.9839676
300	0.8226	0.007658	0.000898	24.154444	5.205504	0.9752310
350	0.5944	0.004882	0.000848	54.653295	15.160192	0.9862853
400	0.6256	0.002004	0.000945	60.210765	44.704858	0.9891405
					Average	0.9803236
					STDS	0.0019333
					% STDS	0.20

----------B.-Cutoff Energy =9keV---------- Attn. B.

Zone (mg/cm^2)	r2Coef. of Det.	a0	sigma a0	a1	sigma a1	
50	0.9715	0.089908	0.003605	19.767385	2.307678	0.9762672
100	0.9703	0.064843	0.002885	24.429552	2.162304	0.9772394
150	0.9398	0.038455	0.002374	22.37783	2.618890	0.9756616
200	0.8844	0.023208	0.001817	21.832673	3.422403	0.9744822
250	0.8738	0.018841	0.001715	34.63444	5.186618	0.9769788
300	0.7556	0.009124	0.000908	23.108184	4.080491	0.9691533
350	0.7452	0.004793	0.000643	35.967367	8.127513	0.9795401
400	0.2644	0.001705	0.000706	40.247829	25.135691	0.9861781
					Average	0.9769376
					STDS	0.0016953
					% STDS	0.17

Attn. Bon (A and B averaged)

n =0.9786 ± 0.0013

REFERENCES

Archard, G.D. 1961. Back Scattering of Electrons. J.Appl. Phys. Vol 32, No. 8, pp. 1505-1509.

Andreo, P. 1991. Monte Carlo Techniques in Medical Radiation Physics. Phys. Med. Biol. 36, pp. 861-920.

Attix, F.H. 1986. Introduction to Radiological Physics and Radiation Dosimetry. New York: John Wiley and Sons, Inc.

Baily, N.A. 1980. Electron Backscattering. Med. Phys. Vol. 7, No. 5, pp. 514-519.

Berger, M.J. 1963. Monte Carlo Calculation of the Penetration and Diffusion of Fast Charged Particles in Methods in Computational Physics Vol.1. edited by B. Alder, S. Fernbach, M. Rotenberg New York: Academic Press, pp.135-215.

Berger, M.J. 1970. Beta-ray Dosimetry Calculations with the Use of Point Kernels. Medical Radionuclides: Radiation Dose and Effects, USAEC Report, pp. 63-86.

Berger, M.J. 1971. Distribution of Absorbed Dose Around Point Sources of Electrons and Beta Particles in Water and Other Media. J. Nucl. Med. Supplement No.5,pp. 5-23.

Berger, M.J. 1973. Improved Point Kernels for Electron and Beta Ray Dosimetry. Report NBSIR-73-107, Nat. Bur. Standards, Gaithersburg MD.

Berger, M.J. and S.M. Seltzer 1982. Stopping Powers and Ranges of Electrons and Positrons, second edition. Washington, D.C.: U.S. Department of Commerce, National Bureau of Standards.

Berger, M.J. 1991. Differences in the Multiple Scattering of Positrons and Electrons. Appl. Radiat. Isot. Vol. 42, No. 10, pp.905-916.

Berger, M.J. and R. Wang 1988. Multiple-Scattering Angular Deflections and Energy-Loss Straggling in Monte Carlo Transport of electrons and Photons, edited by T.M. Jenkins, W.R. Nelson and A. Rindi. New york: Plenum Press.

Bialobzyski, P.J. 1987. Electron Dose Distribution Near Planar Tissue-Bone Interface. MSc. Project Report, McMaster University-Hamilton.

Bevington, P.R. and D.K. Robinson 1992. Data Reduction and Error Analysis for the Physical Sciences, second edition. New York: McGraw-Hill, Inc.

Chibani, O. 1995. Electron Dose Distributions from Point Sources in water, Aluminum, Iron and Lead. Appl. Radiat. Isot. Vol. 46, No. 12, pp.1317-1331.

Cross, W.G. 1967. The Distribution of Absorbed Energy from a Point Beta Source. Can. J. Physics Vol 45, pp. 2021-2040.

Cross, W.G. 1968. Variation of Beta Dose Attenuation in Different Media. Phys. Med. Biol. Vol. 13, No 4, pp. 611-618.

Cross, W.G. 1969. Distribution of Absorbed Beta Energy in Solid Media. Can. J. Physics Vol. 47, pp.75-83.

Cross, W.G., N.O. Freedman and O.N. Mainville 1982. Tables of Beta-Ray Dose Distributions in Water, Air and Other Media, AECL Report. AECL-7617, Chalk River, Ontario.

Cross, W.G., N.O Freedman, and P.Y. Wong, 1992. Tables of Beta-Ray Dose Distributions in Water, AECL Report. AECL-10521, Chalk River, Ontario.

Evans, R.D. 1955. The Atomic Nucleus. New York: McGraw-Hill Book Co., Inc.

Greville, T.N. 1969. Theory and Application of Spline Functions. New York: Academic Press.

Halbleib, J.A. and T.A. Mehlhorn 1984. ITS: The Integrated Tiger Series of Coupled Electron/Photon Monte Carlo Transport Codes, Sandia Report. SAND84-0573, Sandia National Laboratories, Sandia, New Mexico.

Halbleib, J.A 1988. Structure and Operation of the ITS Code System in Monte Carlo Transport of electrons and Photons, edited by T.M. Jenkins, W.R. Nelson and A. Rindi. New york: Plenum Press.

ICRU Report 35, 1984. Radiation Dosimetry: Electron beams with Energy between 1 and 50 MeV. International Commission on Radiation Units and Measurements. Bethsda MD 20814, U.S.A.

ICRU Report 37, 1984. Stopping Power for Electrons and Positrons, International Commission on Radiation Units and Measurements. Bethsda MD 20814, U.S.A.

Loevinger, R. 1950. Distribution of Absorbed Energy Around a Point Source of Beta Radiation. Science Vol.112, pp.530-531.

Loevinger, R. 1954. The Dosimetry of Beta Radiations. Radiology Vol. 66, pp. 74-82.

Loevinger, R. 1956. The Dosimetry of Beta Sources in Tissue. The Point Source Function. Radiology Vol. 66, pp. 55-62.

Kase, K.R. and Nelson, W.R. 1978. Concepts of Radiation Dosimetry. New York: Pergamon Press.

Klevenhagen, S.C. 1991. Implication of Electron Backscattering for Electron Dosimetry. Phys. Med. Biol. Vol. 36, No.7, pp. 1013-1018.

Knoll, G.F. 1989. Radiation Measurement and Detection, second edition. New York: John Wiley & Sons.

Köhler, G. and C. Milstein. 1975. Continuous Cultures of Fused Cells Secreting Antibody of Predicted Specificity. Nature 256, pp. 495-497.

Kwok, C.S., M. Irfan, M. K. Woo and W.V. Prestwich, 1987. Effect of Tissue Inhomogeneity on Beta Dose Distribution of 32P. Med. Phys. Vol 14, No.1, pp.98-104.

Kwok, C.S., P.J. Bialobzysky, S.K. Yu and W.V. Prestwich, 1990. Effect of Tissue Inhomogeneity on Dose Distribution of Point Sources of Low Energy Electrons. Med. Phys. Vol 17, No.5, pp.786-793.

Mausner, L.F. and S.C. Srivastava 1992. Selection of Radionuclides for Radioimmunotherapy. Med. Phys. Vol.20, No.2,pp.503-508.

Mladjenoviç, M. 1973. Radioisotope and Radiation Physics, An Introduction. New York: Academic Press.

Nunes, J.C., W.V. Prestwich, C.S. Kwok, 1993. An Evaluation of the EGS4 And CYLTRAN Monte Carlo Codes with Regard to Boundary Beta-Ray Dosimetry by Comparison with Experimental Beta-Ray dose Backscatter Factors. Med. Phys. Vol.20, No.4, 1250.pp.1243-

Nunes, J.C. 1991. Boundary Electron and Beta Dosimetry - Quantification of the Effects of Dissimilar Media on Absorbed Dose. PhD Thesis, McMaster University - Hamilton.

Patel, S.B. 1991. Nuclear Physics - An Introduction. New York: John Wiley & Sons.

Prestwich, V.W., L.B. Chan and C.S. Kwok 1985. Dose Point Kernels for Beta-Emitting Radioisotopes in Proceeding of the Fourth International Radiopharmaceutical Dosimetry Symposium. Oak Ridge, TN.

Prestwich, V.W., J. Nunes and C.S. Kwok 1989. Beta Dose Point Kernels for Radionuclides of Potential Use in Radioimmunotherapy. J. Nucl. Med. Vol. 30,pp.1036-1046.

Radzievsky, G.B., N.A. Komarov, A.N. Glagolev and E.R. Shepeleva 1980. Distributions of Absorbed Energy from Beta-Radiation in Homogeneous Media. Int. J. Appl. Radiat. Isot. Vol.31,pp. 431-436.

Radzievsky, G.B. and N.A. Komarov 1982. Dose Distributions from Beta-Radiation in Heterogeneous Media: "Two-Group" Method Of calculation. Int. J. Appl. Radiat. Isot. Vol.33,pp. 733-743.

Raylman, R.R. and R.L. Wahl 1995. Magnetically Enhanced Protection of Bone Marrow from Beta Particles Emitted by Bone-Seeking Radionuclides: Theory of Application. Med. Phys. Vol.22, No.8, pp. 1285-1292.

Rogers, D.W. and A.F. Bielajew 1990. Monte Carlo Techniques Of Electron and Photon Transport for Radiation Dosimetry in The Dosimetry of Ionizing Radiation Vol.III, edited by K.R. Kase, B.E. Björngard and F.H.Attix. San Diego: Academic Press.

Snyman, G.C. and C.G. Clayton 1963. Some Observations on the Scattering of Beta-Particles by Thick absorbers. Int. J. Appl. Radiat. Isot. Vol. 14, pp.183-188.

Späth, H, 1974. Spline Algorithms for Curves and Surfaces. Winnipeg: Utilitas Mathematica Publishing Inc.

Spencer, L.V. 1955. Theory of Electron Penetration. Phy. Rev. Vol. 98, No.6, pp.1597-1615.

Seltzer, S.M. 1991. Electron-Photon Monte Carlo Calculations: The ETRAN Code. Appl. Radiat. Isot. Vol. 42, No. 10, pp. 917-941.

Tabata, T. and I. Rinsuke 1992. Simple Calculation of the Electron-Backscatter Factor. Med. Phys. Vol. 19, No. 6, pp. 1423-1426.

Tsoulfanidis, N. 1983 Measurement and Detection of Radiation. New York: McGraw-Hill Book Company.

Yu, S.K. 1989. Dosimetry of Electron Near Planar tissue Interfaces. MSc Project, McMaster University - Hamilton.

Zerby, C.D. and F.L. Keller 1967. Electron Transport Theory, Calculations and Experiment. Nuclear Science and Engineering, Vol. 27, pp. 190-218.

3234 38